BIOFUNCTIONALIZATION OF SUPERPARAMAGNETIC IRON OXIDE NANOPARTICLES

A THESIS

SUBMITTED TO THE MATERIALS SCIENCE AND NANOTECHNOLOGY

PROGRAM OF GRADUATE SCHOOL OF ENGINEERING AND SCIENCE

OF BILKENT UNIVERSITY

IN PARTIAL FULFILLMENT OF THE REQUIREMENTS

FOR THE DEGREE OF

MASTER OF SCIENCE

By

SELİM SÜLEK

July, 2011

I certify that I have read this thesis and that in my opinion it is fully adequate, in scope and in quality, as a thesis of the degree of Master of Science.

……

Prof. Dr. Salim Çıracı (Advisor)

I certify that I have read this thesis and that in my opinion it is fully adequate, in scope and in quality, as a thesis of the degree of Master of Science.

…….

Assist. Prof. Dr. Mustafa Özgür Güler (Co-Advisor)

I certify that I have read this thesis and that in my opinion it is fully adequate, in scope and in quality, as a thesis of the degree of Master of Science.

…….

Prof. Dr. Engin U. Akkaya

I certify that I have read this thesis and that in my opinion it is fully adequate, in scope and in quality, as a thesis of the degree of Master of Science.

…….

Prof. Dr. Mahinur Akkaya

Approved for the graduate school of engineering and science:

…….

Prof. Dr. Levent Onural

Director of the graduate school of engineering and science

ABSTRACT

BIOFUNCTIONALIZATION OF SUPERPARAMAGNETIC IRON OXIDE NANOPARTICLES

Selim Sülek

Supervisor: Prof. Dr. Salim ÇIRACI

M.S. in Materials Science and Nanotechnology

July, 2011

Magnetic resonance imaging (MRI) has attracted intensive interest due to its non-invasive monitoring capacity. Gadolinium based contrast agents, most widely used CA, suffer from high level of toxicity and high threshold of detection. Superparamagnetic iron oxide nanoparticles (SPION) based contrast agents (CA) are good alternatives for gadolinium based CAs, since they have extraordinary magnetic properties within nanometer size and relatively low toxicity. Surface active group of SPIONs are mostly responsible for these advantages. In this thesis, we studied biofunctionalization of iron oxide magnetic nanoparticles with variety of peptide molecules for the solubilization and biofunctionalization of SPIONs. Particle synthesis was carried out via two methods: co-precipitation and thermal decomposition and they were compared by means of size and stability. Several characterization methods, such as Fourier Transform Infrared Spectroscopy (FT-IR), Circular Dichroism (CD), Rheology, X-ray diffraction (XRD) X-ray photon spectroscopy (XPS), vibrating

sample magnetometer (VSM), Magnetic resonance imaging (MRI), Atomic Force Microscopy (AFM), Scanning Electron Microscopy (SEM), Transmission Electron Microscopy (TEM) were used in order to fully characterized the SPIONs prepared.methods were used in order to fully characterize the SPIONs. Thermal decomposition is the best method to control the particle size and avoid aggregation problems. Peptide amphiphile molecules are used to non-covalently functionalize SPIONs synthesized by thermal decomposition method to provide water solubility and biocompatibility. Particles are found to be around 35 nm with r_2 values of 100.4 and 93.7 $s^{-1}mM^{-1}$ which are comparable with commercially available SPIONs. *In vitro* cell culture experiments revealed that peptide-SPION complexes are biocompatible and are localized around the cells due to their peptide coating. Finally, SPIONs were evaluated in terms of their potential use as MRI contrast agent.

Keywords: Magnetite, maghemite, MRI, superparamagnetic, bioactive, peptide amphiphile, iron oxide, contrast agent, non-covalent interactions, thermal decomposition, co-precipitation.

ÖZET

SÜPERPARAMANYETİK DEMİR OKSİT NANOPARÇACIKLARIN BİYOİŞLEVSELLEŞTİRİLMESİ

Selim Sülek

Malzeme Bilimi ve Nanoteknoloji Programı, Yüksek Lisans

Tez Yöneticisi: Prof. Dr. Salim ÇIRACI

Temmuz, 2011

Manyetik rezonans görüntüleme tekniği sunduğu invazif olmayan görüntüleme kapasitesi nedeniyle büyük ilgi çekmektedir. Manyetik rezonans görüntüleme tekniğinde istenilen dokunun görüntülenmesi için kontrast ajanları kullanabilmektir. Yaygın olarak kullanılan gadolinyum tabanlı kontrast ajanları, yüksek toksik özellikler ve de yüksek deteksiyon seviyeleri nedeniyle eleştirilmektedirler. Süperparamanyetik demir oksit nanoparçacık tabanlı kontrast ajanları, sahip oldukları nanometre ölçeğinde gösterdikleri üstün manyetik kuvvet ve düşük toksik özellikleri sayesinde gadolinyum tabanlı kontrast ajanlarına güzel bir alternatiftirler. Parçacıkların yüzeyinde bulunan aktif biyoaktif moleküller bu avantajların sağlanmasında büyük rol oynamaktadır. Sunulan bu çalışmada, demir oksit nanoparçacıklarının ko-presipitasyon ve termal dekompozisyon yöntemleri ile sentezlenmesi ve

yüzeylerinin fonksiyonalizasyonu gösterilmiştir. Elde edilen parçacıklar Fourier Transform Kızılötesi Spektroskopisi (FT-IR), Circular Dichroism (CD), Reoloji, X-Işını Saçılım Spekroskopisi (XRD), X-ray fotoelektron spektroskopisi (XPS), titreşimli örnek manyetometresi (VSM), manyetik rezonans görüntüleme tekniği (MRI) Atomik Kuvvet Mikroskopu (AFM), Taramalı Elektron Mikroskopu (SEM), Geçirmeli Elektron Mikroskopu (TEM) ile elde edilmiş ayrıca sentezlenen parçacıkların biyolojik örnekler ile etkileşimi incelenmiştir. ile karakterize edilmiş ve sentezlenen parçacıkların biyolojik örnekler ile etkileşimi incelenmiştir. Elde edilen sonuçlara göre termal dekompozisyon yöntemi hem parçacık büyüklüğünün kontrolü hem de topaklaşmanın önlenmesi için en uygun yöntemdir. Termal dekompozisyon yöntemi ile sentezlenmiş parçacıkların kaplanması için amfifilik peptitler kullanılmıştır. Hidrofobik etkileşim prensibine dayanan bu yöntem ile parçacıklara suda çözünebilirlik ve biyoaktiflik kazandırılmıştır. Sentezlenen parçacıklar 35 nm civarlarında olup r_2 değerleri 100.4 ve 93.7 $s^{-1}mM^{-1}$ olduğunu göstermektedir. Elde edilen in vitro sonuçlara göre parçacıkların biyouyumlu olduğu ve hücrenin çevresinde toplandığı gözlemlenmiştir. Sentezlenen parçacıkların MRI contrast ajanı kullanımı MR aletiyle ölçülmüştür.

Anahtar Sözcükler: Manyetit, maghemit, MRI, süperparamanyetik, biyofonksiyonel, amfifilik peptid, demir oksit, kontrast ajanı, kovalent olmayan etkileşimler, termal dekompozisyon, ko-presipitasyon.

ACKNOWLEDGMENT

I would like to express my gratitude to my supervisor Assist. Prof. Dr. Mustafa Özgür Güler for his guidance in this research.

I would like to thank to Büşra Mammadov and Davut İbrahim Mahçiçek for their partnership in this research.

I would like to express my special thanks to Assist. Prof. Dr. Ayşe Begüm Tekinay, Prof. Dr. Ergin Atalar, Assoc. Prof. Dr. Hüseyin Sözeri, Assoc. Prof. Dr. Muhammet Toprak and Assoc. Prof. Dr. Aykutlu Dâna for their support and sharing their knowledge.

I want to thank to my group members Rukan Genç, Handan Acar, Ruslan Garifullin, Sıla Toksöz, Turan Selman Erkal, Zeliha Soran, Oya Ustahüseyin, Okan Öner Ekiz and Adem Yıldırım. It was wonderful to work with them.

I would like to thank to UNAM (National Nanotechnology Research Center) and TÜBİTAK (The Scientific and Technological Research Council of Turkey) grant number 109S386 for financial support, UMRAM (National Institute of Magnetic Resonance Imaging) and UME (National Metrology Institute) for help with characterizations.

Dedicated to

My dearest Family

LIST OF ABBREVIATIONS

PA: Peptide Amphiphile

MRI: Magnetic Resonance Imaging

SPION: Superparamagnetic iron oxide nanoparticles

IOP : Iron Oxide Nanoparticles

T1: Longitudinal Relaxation

T2: Transversal Relaxation

FMOC: 9-Fluorenylmethoxycarbonyl

HBTU: 2-(1H-Benzotriazol-1-yl)-1,1,3,3-tetramethyluronium hexafluorophosphate

DIEA: N, N-Diisopropylethylamine

DMF: Dimethylformamide

TFA: Trifluoroacetic Acid

TIS: Triisopropylsilane

MTBS: Mono-*tert*-Butyl Succinate

APTES: (3-Aminopropyl)triethoxysilane

$Fe(acac)_3$: Iron (III) acetylacetonate

LC-MS: Liquid Chromatography-Mass Spectrometry

AFM: Atomic Force Microscopy

TEM: Transmission Electron Microscopy

FT-IR: Fourier Transform Infrared Spectroscopy

SEM: Scanning Electron Microscopy

CA: Contrast Agent

VSM: Vibrating Sample Magnetometer

XRD: X-Ray Diffraction Spectroscopy

DLS: Dynamic light Scattering

r_2: Transverse relaxivity

r_1: longitudinal relaxivity

Mag-TE: Magnetic Tissue Engineering

M_s: Magnetic Saturation

TABLE OF CONTENTS

LIST OF FIGURES

LIST OF TABLES

CHAPTER 1

INTRODUCTION

1.1. INTRODUCTION

Nanomedicine stands at the boundaries of physics, chemistry and biology, and the progress in nanotechnology makes nanomedicine more operational in real life. From a point of view, nanomedicine consists of the applications of materials and systems in nanometer size for therapeutic applications, diagnosis and sensing applications. Nanomedicine has certain advantages over the traditional approaches. The small and controllable size of the nanoparticles enables the investigation of cells or tissues more precisely[1].

Compared to bulk materials, nanometer-sized materials exhibit different physicochemical properties. Among different categories of nanomaterials, iron oxide nanoparticles (IOP) attracted intense interest for biological applications because of their unique physicochemical properties. One of those properties of IOP is their superparamagnetic feature which helps to overcome some bottlenecks in medicine as depicted in Figure 1.[2] Another important physicochemical property of the IOP is the size, shape and constituent of the particles. IOP consist of biocompatible and biodegradable iron ions. Nanoparticle size can be controlled over a few nanometers to tens of nanometers. Also the shape of the nanoparticles can vary (e.g. sphere,

cube or nanotube). Size of the IOP could be smaller than or comparable to a living cell (10-100 μm), virus (20-450 nm), or a protein (5-50 nm).

As these data clearly present that magnetic nanoparticles are able to interact with biological matter with appropriate coating, and this makes SPIONs important tools for medical approaches. There are numerous types of coating group for magnetic nanoparticles including polymers, silica, protein, peptides, nucleotides [1,3,4].

Briefly, the use of IOP in medicine depends on their superparamagnetic feature, synthesis pathway and surface active groups.

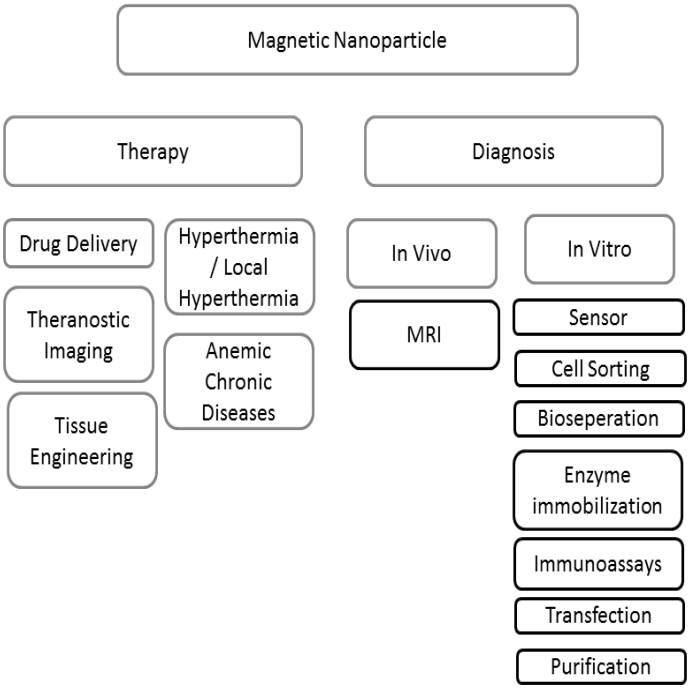

Figure 1. Biomedical Applications of Magnetic Nanoparticles.

1.2. Superparamagnetism

Broadly, all materials can be called as magnetic materials because almost all materials to some extent can response to the magnetic fields. [3,4] However, they are classified based on their volumetric magnetic susceptibility, χ, which describes the relationship between the magnetic field H and magnetization M induced in a material by the magnetic field [3,4] :

$$M = \chi H \qquad 1.1$$

Some materials contain unpaired electrons. These electrons could be coupled with neighboring atoms. In the absence of an external field, this interaction results in spontaneous magnetization, and retains the alignment imparted by an applied field after the field has been removed. This behavior is called as *ferromagnetic* or *ferrimagnetic* which is also called as *magnetic* in daily life [1,3,4]. Figure 2 demonstrates ferromagnetic particles. A ferromagnetic material that has never magnetized or demagnetized will follow the dashed line as H is increased. At point a, it reaches its magnetic saturation point where all magnetic domains are aligned. When current reduces to zero, it will reach to the point b, which is called as *retentivity point*. This point indicates the level of the residual magnetism in the material. At that point, the magnetic domain alignments remain the same whereas some of them lost their alignment. If magnetization force is reversed, the curves will reach to the coercivity point which is pointed as c. Coercivity point represents the reversed magnetizing force which demagnetizes the materials. At that point magnetic alignment will be lost

and electrons will be distributed randomly. As magnetic force applied in the negative direction, it will reach the point d which is again saturation point likewise the point a [5]. In superparamagnetic materials, both coercivity and retentivity values are equal to zero at room temperature as seems in Figure 3. In other words, superparamagnetic materials loose magnetic alignment so their magnetic properties lost once the magnetic field removed. This unique property avoids magnetic agglomeration which dramatically affects the biological use [5].

As shown in equation 1, response of the magnetic materials to the magnetic field is directly affected by magnetic susceptibility of the material. There are several important parameters affecting the magnetic susceptibility of SPIONs, such as their size, shape, crystallinity (phase) as well as their constituents and surfactant groups. All these parameters have to be taken into account during the synthesis in order to get better magnetic susceptibility [3,6].

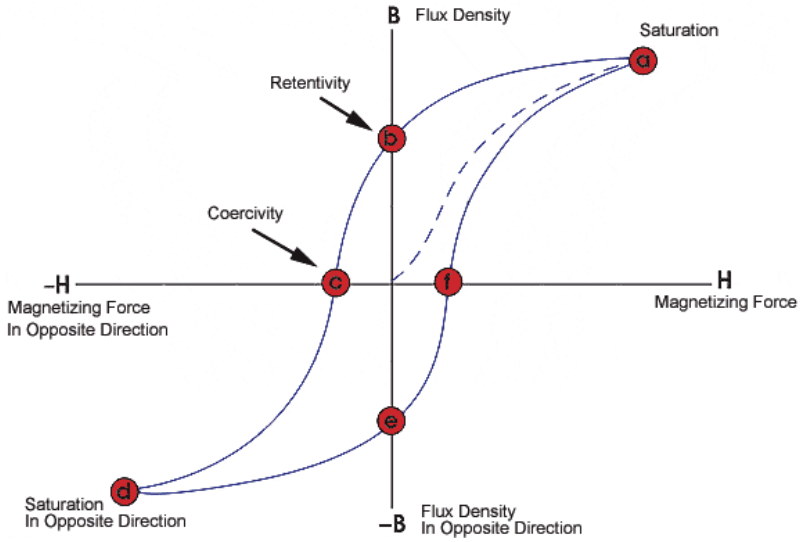

Figure 2. A typical hysteresis loop of magnetic materials. Picture is adapted with permission from NDT group [5]

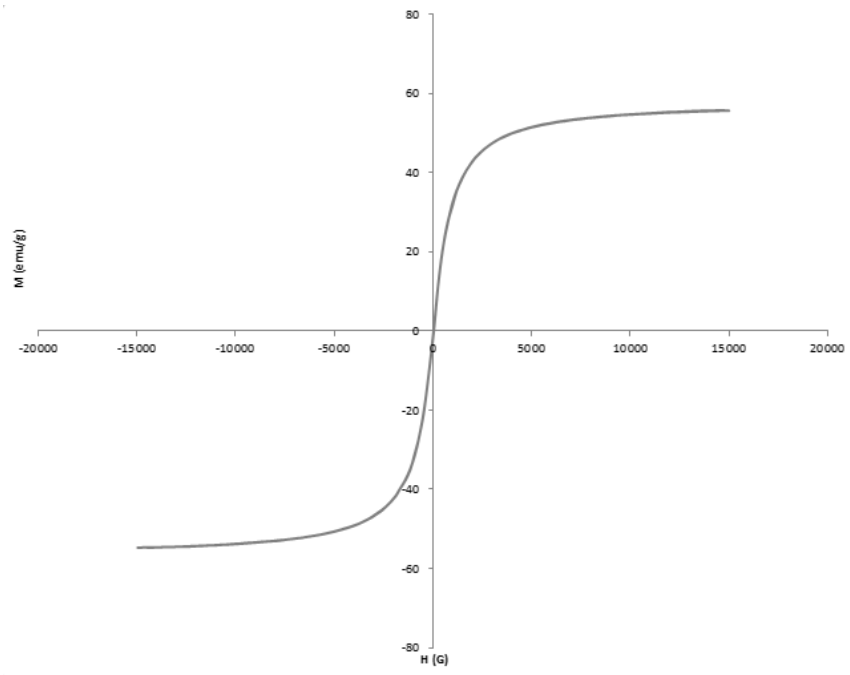

Figure 3. Hysterysis loop of superparamagnetic materials. When a magnetic field applied to superparamagnetic materials, the hysterysis follows a similar pattern within positive and negative direction.

1.3. Synthesis of SPIONs

Numerous methods have been developed to synthesize magnetic nanoparticles, and the most wildly used examples are sonochemical reactions, co-precipitation reactions, hydrothermal reactions and thermal decomposition [7,8].

Co-precipitation technique is probably the simplest and most efficient way to obtain SPIONs. They usually prepared by aging in basic solution with 2:1 stoichiometric mixture of $FeCl_3$ and $FeCl_2$ respectively in non-oxidizing nature. Chemical reaction of magnetite (Fe_3O_4) formation could be written as:

$$Fe^{2+} + 2Fe^{3+} + 8OH^- \xrightarrow{yields} Fe_3O_4 + 4H_2 \qquad 1.2$$

Magnetite (Fe_3O_4) has higher magnetic saturation then other IOP phases such as maghemite, hematite or goethite. However, they are not stable by means of crystallinity and can be transformed into other phases of iron oxide in the presence of oxygen.

$$Fe_3O_4 + 2H^+ \xrightarrow{yields} \gamma Fe_2O_3 + Fe^{2+} + H_2O \qquad 1.3$$

Co-precipitation is advantageous due to the fact that it is an easy method and allows large amount of nanoparticles synthesis. However, the limited control over synthesis is a drawback where only the kinetic factors are in charge during the growth of crystals as stated by Lamer [7-9].

LaMer diagram shown in Figure 4 reveals formation of monodisperse nanoparticles with the nucleation and the crystal growth mechanisms in three consecutive phases. In phase I, monomer concentration increases up to its saturation point. In phase II, monomer concentration reaches its supersaturation point where it has enough energy to overcome energy barrier and eventually nuclei are formed simultaneously. That will end up with a dramatic decrease in the nucleation until no further nucleation is possible. Nuclei grow comes to an end in phase III, and the control over nucleation step could determine the size and size distribution and the shape of SPIONs. pH adjustment, ionic strength, temperature, nature of salts, the Fe^{II}/Fe^{III} concentration ratio, existence of oxygen, injection fluxes, temperatures, iron and solvent concentration are the critical factors have to be taken into consideration for a well-controlled synthesis of SPIONs [9].

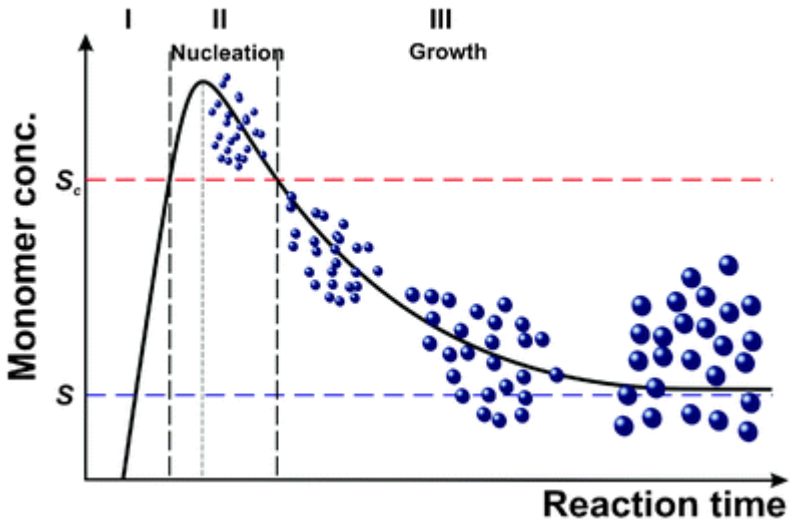

Figure 4. LaMer plot illustrating the nucleation and growth during the synthesis. Picture is adapted with permission from references [9]. The nucleation process rapidly occurs with a subsequent nuclei formation. This simultaneous formation ends up with aggregated particles of different core sizes.

Another important synthesis method is hydrothermal synthesis. Reactions are performed in the aqueous media in autoclave where the pressure can be higher than 2000 psi and the temperature can reach above 200 ºC. In hydrothermal reactions, particle size can be tailored simply by temperature where ultrafine SPIONs can easily be synthesized [7,8].

Thermal decomposition method is the best method to control the size and monodispersity of the synthesized nanoparticles. For many variations of thermal decomposition method, many different solvents and surfactants are used. Numerous types of thermal decomposition method have been developed. Sun et al. described a high temperature mediated reaction of $Fe(acac)_3$ with 1,2-hexadecanediol in the presence of oleic acid and oleylamine. Resulting nanoparticles were monodisperse and size could be tuned from 4 nm to 20 nm [10]. Size of the SPIONs synthesized using thermal decomposition method depends strongly to reaction temperature, iron to surfactant ratio and reaction time which are easily controllable. SPIONs synthesized by thermal decomposition method is soluble in organic solvents because SPIONs are stabilized and protected from aggregation by surfactant surface coating through the polar head group of the surfactant attached to the hydrophobic tail extending away from the SPIONs as shown in Figure 5 [3,4,7,8,10].

There are several other methods to synthesize SPIONs. One of the key parameter for medical usage is their surface active group. Surfactant is needed for the stabilization, water solubility and bio-applications.

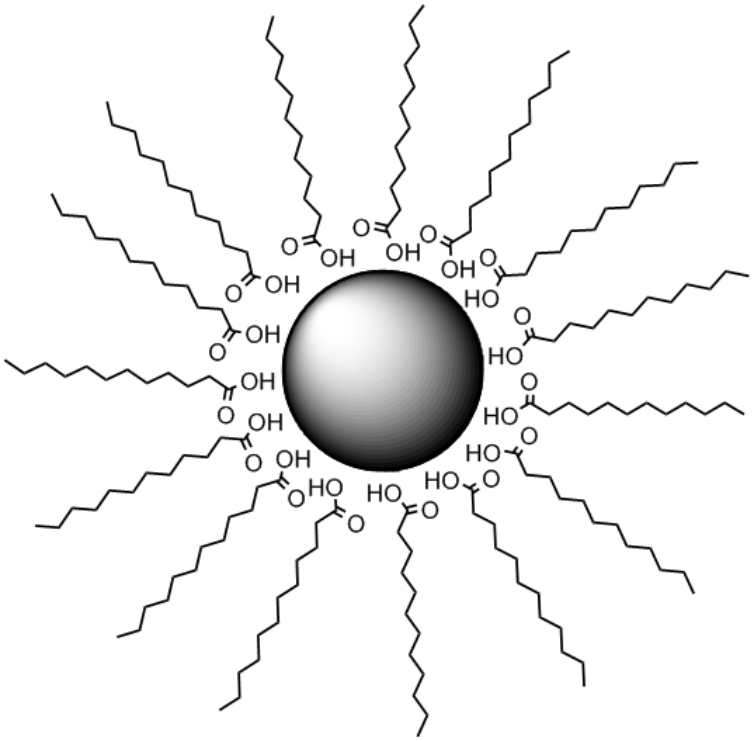

Figure 5. A schematic representation of SPIONs synthesized by thermal decomposition method. Lauric acid coated the SPION surface during the synthesis.

1.4. Surface Modification of SPIONs

Functionalization of SPIONs' surface represents an indispensable step for the biological applications. Physicochemical and biological properties of

SPIONs can be tailored with their surface active groups [11]. In the absence of any surfactant, SPIONs tend to agglomerate due to a physical phenomenon explained by DLVO theory [12].

DLVO theory suggests that stability of a particle is dependent upon its total potential energy function V_T. According to the theory, V_T is the balance between several factors which are solvent potential energy V_s, attractive forces V_A and repulsive forces V_S :

$$V_T = V_S + V_R + V_A \qquad 1.4$$

According to DLVO theory, stability of the colloidal nanoparticles determined by the balances between the Van der Waals (V_A) and electrical double layer repulsive (V_R) forces exist between nanoparticles. If the repulsive forces between the particles are sufficient, the dispersion will resist to flocculation and it will stabilized the colloidal nanoparticles [13]. Herein, bare nanoparticles have not sufficient repulsive forces so that eventually aggregation takes places [14].

Moreover, in the presence of salts or any other electrolytes in the biological media, electrostatic stabilization arising from the SPIONs' surface charge falls behind the adequate level to overcome the attractive forces between two NPs and leads larger aggregates which can easily be removed by reticuloendothelial system and/or by opsonization [14].

The most applied surfactant types for steric stabilization of particles are polymers [7]. Polymers can provide stability against agglomeration and

opsonization. Also it provides surface groups which can be used for biological functionalization of NPs with proteins, peptides and hyaluronic acids. Poly(ethylene glycol) and dextran are most common polymer types for not only coating of SPIONs but also all nanoparticles due their high biocompability. Poly(ethylene glycol) also reveals antifouling properties that reduces their uptake by macrophages and extends their blood circulation time [15].

Another trend for the SPION functionalization is the core-shell structure [16]. These core-shell structures offer a potential in such areas as theranostic imaging, delivery agent and sensor applications, better biocompatibility, and better stability in aqueous solutions [1,4].

First and the most common core shell structures are SPION core silica shell structures in which silica comes with some advantages, such as better biocompatibility, easy coating process, chemical inertness and optical transparency as well as better stability in aqueous solutions and controlled porosity. The thickness of the silica coat can be tuned in a range of 10-100 nm by varying the concentration of ammonium and the ratio of tetraethoxysilane (TEOS) which have unique porous structure. Controlled porosity of the resulting structure offers some advantages in encapsulation of other molecules like drugs, inorganic nanoparticles and dyes within the complex. These encapsulated nanoparticles can be promising tools with a potential use in dual imaging and/or theranostic applications [17].

Other core-shell structures are metals/metal oxides. These SPIONs core-shell structure can offer semiconducting, plasmonic, specific affinity and magneto-optical properties. For that purposes SPIONs can be coated with gold, TiO_2, CdSe and/or CdTe. These structures can especially be used for biosensor applications [16].

1.5. Applications of SPIONs in Medicine

SPIONs offer some attractive possibilities in medicine and come up with several advantages. The first advantage is the controllable size of SPIONs ranging from a few nanometers up to tens of nanometers. This feature led them to be close to biological entities which are in same dimension in size perspective. Another important point is that SPIONs can be manipulated by an external magnetic field. This action at a distance feature can be combined with many applications such as MRI, delivery vehicles, therapeutic applications, theranostic applications, sensor applications, tissue engineering applications and purification & isolation applications [1].

1.5.1. MRI

MRI is one of the most powerful non-invasive imaging techniques in clinical use. Its basic principle is the measurement of the relaxation of protons in an external magnetic field after the radio-frequency pulse excitation [18].

When nuclei placed in a magnetic field, randomly oriented nuclei tend to align either in the same or opposite direction of the magnetic field and

there is no overall magnetic vector in the XY plane as represented in Figure 6-a. After radiofrequency excitation with a 90º, the spin up and spin down states are equalized resulting in a zero m_z as represented in Figure 6-b and the magnetization is maximum in the perpendicular XY plane. There are two forms of relaxation from this excited state; transversal relaxation and longitudinal relaxation.

Over the time, as represented in Figure 6-c, the magnetization in XY plane decreases and returns to the magnetic field direction, and an energy release to the environment occurs (lattice). This process is called longitudinal (or spin-lattice) relaxation.

Another loss type of magnetization in XY plane is transverse relaxation. After the excitation, all spins are localized on the XY plane. There can be energy exchange between spins at that step which induced by a local magnetic field and this relaxation is called transverse (spin-spin) relaxation. A representative graphic can be seen in Figure 6-d.

As mentioned before, MRI is one of the most powerful methods for medical diagnosis owing to its non-invasive process, high spatial resolution multidimensional tomographic capabilities dynamic and functional monitoring capabilities. This enormous versatility and functionality of MRI has led to huge demand in medical diagnosis of abnormal tissues and organs [1,3,18].

From the perspective of medicine; the contrast in MRI arises from the physicochemical interaction between water and tissues; hence this technique

is not only sensitive to the amount of water but also to the concentration of any molecule in the tissue. However, this technique suffers from low-signal sensitivity which can be overcome by the use of contrast agents. MRI contrast agents improve the image quality by altering the T_1 or T_2 relaxation times of water nearby. Gd^{3+} based paramagnetic contrast agents are the most commonly used contrast agents and provide good positive contrast. SPIONs are good alternatives for Gd^{3+} based contrast agents. Firstly, SPIONs are much more efficient contrast agents then the Gd^{3+}. The main reason for that is the difference between their relaxivities. While Gd^{3+} complexes` r_1 is around 10 $mM^{-1}s^{-1}$ whereas r_2 values of SPIONs are around 80-100 $mM^{-1}s^{-1}$. Also SPIONs comes up with some other advantages such as biocompatibility and biodegradability [1,14,15,19].

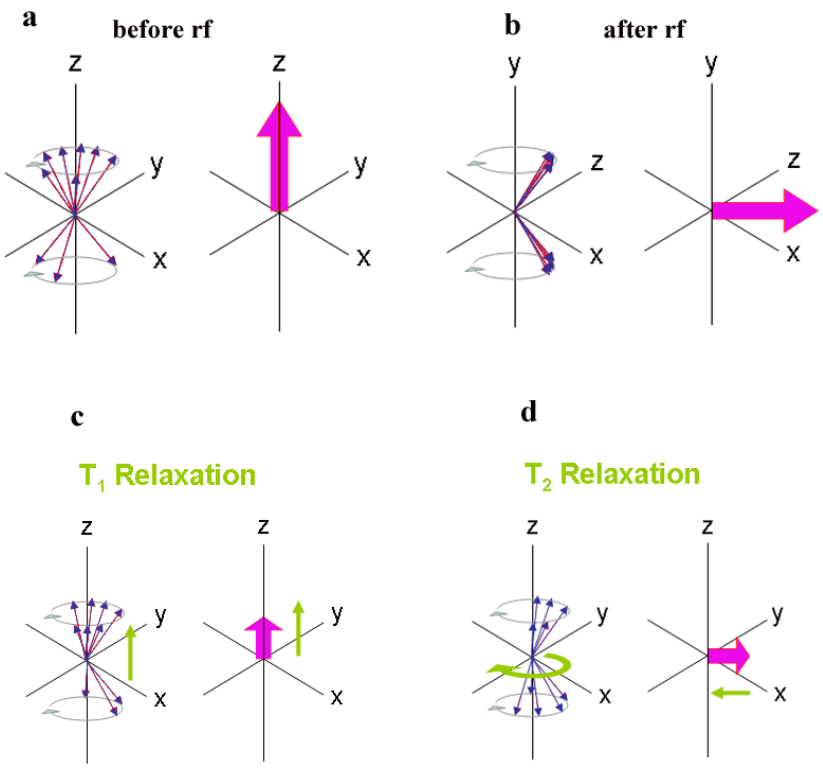

Figure 6. Schematic representation of MRI working principles a) vector distribution of nuclei when magnetic field applied b) vector drawing of nuclei after radiofreuency pulse applied c) vector drawing of nuclei in T_1 relaxation state d) vector drawing of nuclei in T_2 relaxation state. Picture is adapted with permission from EMRIC [20].

1.5.2. Magnetic Tissue Engineering

It is well-known that mechanical forces influence cellular functions. The differentiation of stem cells can be controlled by mechanical forces. In magnetic concept, remote control of mechanotrunsduction leads to development in magnetic tissue engineering applications. Use of SPIONs in tissue engineering has increased demand. They can be used to guide cell

adherence locations. Since SPION labeled cells can be manipulated by a magnet, a novel methodology for cell seeding in 3-D scaffold could be possible via magnetic guidance. In conventional cell seeding methods, cell suspension is seeded into small scaffolds using small volumes of highly concentrated cell suspension. The problem in here is that the seeded cell suspension flow away and very few cells remain in the scaffold. Mag-Te could help to overcome this problem via magnetic attraction.

Mag-Te have been used in various tissue types such as bone and cartilage, blood vessels, skin, lung, eye, liver, and nervous tissue. Mag-Te is undergoing a rapid expansion in tissue engineering applications. The ability to manipulate cellular process remotely will open myriad opportunities in tissue engineering Also SPIONs can also be used to monitor cellular movement *in vivo* by MRI [1].

CHAPTER 2

EXPERIMENTAL SECTION

2.1 General Methods

SPIONs were characterized by Panalytical X'PERT Pro MRD model XRD and their magnetic behavior was examined by the vibrating sample magnetometer (LDJ, Electronics Inc., Model 9600) with maximum field up to 15 kOe. Reverse phase HPLC on Agilent 6530 accurate-Mass Q-TOF LC/MS equipped with Agilent 1200 HPLC was used to characterize the peptide amphiphiles. Agilent Zorbax Extend-C18 2.1 x 50 mm column for basic conditions and Zorbax SB-C8 4.6 mm x 100 mm column for acidic conditions were used to analyze peptides. A gradient of (a) water (0.1% formic acid or 0.1% NH_4OH) and (b) acetonitrile (0.1% formic acid or 0.1% NH_4OH) was used for the analysis of peptides. For purification of the molecules, reverse-phase HPLC system with Zorbax Extend-C18 21.2 x 150 mm column for negative molecules and Zorbax SB-C8 21.2 x 150 mm column for positive molecules was employed. A gradient of (a) water (0.1% TFA or 0.1% NH_4OH) and (b) acetonitrile (0.1% TFA or 0.1% NH_4OH) was used for the analysis of peptides.

2.2. Materials

Dibenzyl ether was purchased from Merck, lauryl amine was purchased from Sigma-Aldrich, iron 2,4 pentadionate ($Fe(acac)_3$) and lauric acid were purchased from Alfa Aesar. 1,2 hexadecane diol was purchased from Sigma-Aldrich. 9-Fluorenylmethoxycarbonyl (Fmoc) and tert-butoxycarbonyl (Boc) protected amino acids, [4-[α-(2',4'-dimethoxyphenyl)Fmoc-aminomethyl]phenoxy]acetamidonorleucyl-MBHA resin (Rink amide MBHA resin), Fmoc-Asp(OtBu)-Wang resin and 2-(1H-Benzotriazol-1-yl)-1,1,3,3-tetramethyluronium hexafluorophosphate (HBTU) were provided from NovaBiochem and ABCR. NH_4OH, NaOH and HCl were purchased from Riedel-de Haen. $FeCl_3$ was bought from Merck. $FeCl_2$ was bought from Sigma-Aldrich. TFA solution NHS and EDC bought from Merck. The other chemicals were purchased from Fisher, Merck, Alfa Aesar or Aldrich and used as provided.

2.3. Synthesis of Peptides

Positive peptides were constructed on Rink Amide MBHA resin, whilst negative peptides were constructed on preloaded wang resin. Amino acid couplings were done with 2 equivalents of Fmoc protected amino acid, 1.95 equivalents HBTU and 3 equivalents of DIEA for 2 hours. Fmoc removals were performed with 20% piperidine/DMF solution for 20 min. Cleavage of the peptides from the resin was carried out using a mixture of TFA:TIS:H_2O in 95:2.5:2.5 ratio for 2 h. Excess TFA was removed by rotary evaporation.

Remaining viscous peptide solution was treated with ice-cold diethyl ether, and the resulting white pellet was freeze-dried.

2.4. Superparamagnetic Iron Oxide Nanoparticle Synthesis via Thermal Decomposition Method

Magnetite (Fe_3O_4) nanoparticles were synthesized as previously reported with slight modifications in synthesis protocol[10]. 2 mmol $Fe(acac)_3$, 10 mmol 1,2 hexadecane-diol, 6 mmol lauric acid and 6 mmol lauryl amine were dissolved in 20 ml benzyl ether. Solution was then deoxygenated with nitrogen gas and magnetically stirred while heating up to 200 °C for 2 h. Afterwards, resulting solution was refluxed at 270 °C for 1 h and cooled down to room temperature. Subsequently, 50 ml ethanol was added to precipitated nanoparticles. In following step, solution was centrifuged at 8000 rpm for 10 min. Precipitated nanoparticles were collected and dissolved in hexane. More ethanol was added and centrifuged at 8000 rpm for 10 min. The pellet was treated with hexane in the presence of 1 mmol lauric acid, lauryl amine and sonicated for 10 min to recover the NPs. Finally, solution was centrifuged at 6000 rpm for 10 min to remove the aggregated particles.

2.5. Non-covalent Functionalization of Superparamagnetic Iron Oxide Nanoparticles

30 mg of peptide amphiphile was dissolved in 3 ml distilled water and pH of the solution was adjusted to pH 2 and pH 10 for the positive charged

peptide amphiphile and negative charged peptide amphiphile, respectively. Then 10 mg/ml of SPION stock solution in hexane was prepared. Peptide amphiphiles and SPION's were mixed with a ratio of 1:7. 21mg/2.1 ml and peptide amphiphile solution was then sonicated for 5 min and 3 mg/0.3 ml. After pouring SPION solution into the PA solution, mixture was shaken for a couple of seconds and sonicated for 1 min. This step was repeated for 10 min and sonication was performed for 30 min. Further, solution was heated to 60 °C, and vigorously mixed for 20 min more at 60 °C. Then, the solution was filtered through 0.2 μm PTFE filter and centrifuged at 10000 rpm for 90 seconds. Supernatant solution was removed and centrifuged at 12500 rpm for 20 min. Precipitated particles were dissolved in ddH_2O. Free peptide concentration was measured with UV Nano-drop at 205 nm.

2.6. SPION's Surface Modification with APTES

Surface modification was done according to literature [21]. 10 mg SPION was dissolved in 100 ml hexane. 0.5 ml APTES and 10 μL acetic acid solutions were added into hexane solution. Then, the solution was mixed at 120 rpm for three days. It was centrifuged at 8000 rpm for 10 minute and supernatant removed. More hexane added into solution and magnetic particles were separated with magnet. This step was repeated three times more and dissolved in H_2O.

2.7. SPION Synthesis via Co-Precipitation Method

50 ml NH_4OH solution (1 M) was prepared and the pH of the solution was adjusted to pH 11 by adding HCl. Solution was deoxygenated with nitrogen gas for 30 minutes. 0,65g $FeCl_3$ and 0.25g $FeCl_2$ were mixed in 2.5 mL pH 3 solutions with a molar ratio of 2:1. Then, the solution was injected into pH 11 solution under nitrogen gas and sonicated for 1 h. Precipitated particles with black color were collected and centrifuged at 6000 rpm for 10 min and washed three times.

2.8. Protein Conjugation Studies

For the conjugation process, EDC/NHS reaction was applied. 11 mg EDC and 15 mg NHS were mixed in 0.1M MES buffer (pH 5). For the functionalization of Pro-PA(1) and Pro-PA(2) SPION complexes, 200 µL of SPION solution was added into the previously prepared solution and the final solution was shaken overnight. Then, 10X PBS was added to raise the pH and further, FITC labeled streptavidin was added into solution. The mixture was shaken for 3 hours more. For the APTES modified SPIONs, 200 µL of 1 mg/ml biotin solution was mixed with 11 mg EDC and 15 mg NHS in 0.1 M MES buffer and shaken overnight. Subsequently, 10X PBS was added to raise the pH and 200 µL APTES modified SPION solution added into solution of previously prepared NHS/EDC activated biotin.

2.9. Characterization of Iron Oxide Nanoparticles

Dynamic Light Scattering

Hydrodynamic size and zeta potential of the particles were measured by dynamic light scatteringusing Malvern Nanosizer/Zetasizer®nano-ZS ZEN 3600 (Malvern Instruments, USA) instrument. Basically, hydrophobic particles were dissolved in hexane and measurements were performed in a quartz cuvette. The hydrophilic particles were dissolved in water and measurements were performed in a polystyrene cuvette.

X-Ray Diffraction (XRD)

Panalytical X'PERT Pro MRD was used to collect XRD diffraction pattern analysis under Cu Kα radiation. Samples were dried by vacuum and grinded to obtain a fine powder. After that, samples were spread onto glass XRD substrate and analyzed.

FT-IR

Bruker VERTEX 70 with Hyperion Scanning Microscope was used for the FT-IR analysis at the transmittance mode. 1 mg SPION was grinded with 99 mg KBr until very fine powders were obtained. The mixtures were stated between two stainless steel disks and hydraulic press was applied up to 7 atm. Transmittance characterization was done between 370-4000 cm^{-1}.

Scanning Electron Microscopy (SEM)

SEM imaging was performed with FEI Quanta 200 FEG, using the ETD detector at high vacuum mode with 30 keV beam energy. For sample

preparation; 1 mg/ml of sample solutions were drop cast on silicon wafer and dried before sample analysis. Particle morphology was evaluated by comparison of several images taken from diverse sides of the specimen.

Transmission ElectronMicroscopy

TEM was performed with FEI Tecnai G2 F30. Diluted samples were placed on a Lacey mesh ultrathin carbon coated copper grid. In order to observe the organic layer around the SPION, the particles were stained with 2 wt % uranyl acetate solution or phosphotungstic acid solutions for positive and negative staining, respectively. 5μL SPION solution dropped onto grid. Then, the grid was washed to remove excess coating and was put over the staining solution for 15 min. After the staining, the grids were dried at room temperature overnight before further analysis. Particle size and sample uniformity were evaluated by comparison of several images taken from diverse sides of the specimen.

Cell Viability

The effect of synthesized SPIONs on cell viability were analyzed using Mouse embryonic fibroblast cells (NIH 3T3). NIH 3T3 cells were cultured in DMEM supplemented with 10% calf serum. 24 h later, cells were seeded on 96 well-plates (5000 cells/well) containing different concentration of SPIONs (500 μg/ml, 200 μg/ml, 100 μg/ml, 50 μg/ml) (pH 7). Live/Dead assay was used to detect living cells by Calcein AM (2 μM) and death ones by ethidium homodimer 1 (2μM) 48 h after the addition of SPIONs. Fluorescence measurements were taken by M5 microplate reader. Peptides

without iron oxide nanoparticles were used as negative control at same concentrations.

Prussian Blue Staining

Cellular localization and internalization was detected by Prussian Blue staining. NIH 3T3 cells were seeded in 96 well-plates (3000 cells/well). 24 h after seeding the cells, SPIONs were added with the concentration of 500 µg/ml at pH 7. 24 h after the addition of SPIONs, PB staining was performed. Wells were washed using PBS and fixed 4% paraformaldehyde. Fresh mixture of 2% HCl: 2% $K_4Fe[CN]_6$ (1:1) was added on the cells and incubated at room temperature for 30 min. Then wells were washed with PBS and images were taken under inverted microscope (Zeiss).

The iron content of peptide coated SPIONs was quantitatively determined by the colorimetric PB assay and measured by Spectramax M5. Samples were prepared by mixing 200 µl of SPIONs or their diluted solution with 200 µl of 6 N HCl for 1 h at 60 °C. After mixing process 100 µl 5% $K_4Fe[CN]_6$ solution was added. The iron content of samples was calculated by comparing its absorbance (650 nm) to that of a range of standard concentrations of equal volume.

Magnetic Resonance Imaging

MRI measurements of the peptide coated SPIONs were performed on a Siemens 3T TIMTrio Scanner. Peptide coated SPIONs were dispersed in water and diluted to various concentrations (0.0375, 0.075, 0.15, 0.2, 0.5

mM) and pH of the solutions was adjusted to 7. A 5 ml glass sample holder was placed in the iso-center of the magnet. Spin-echo pulse sequences were utilized to obtain T_1 and T_2 maps of each sample. T_1 and T_2 relaxation times were measured from the large regions of interest, and the R_1 and R_2 relaxation rates were obtained from the reciprocal of obtained T_1 and T_2 result. MR imaging capabilities of the SPIONs were examined at 3 T with the following parameters' point resolution: 0.11-0.11 cm, section thickness: 2.3 mm, TE: 11, 13, 15, 18, 20, 30, 50, 100, 200, 500 ms, TR: 3000 ms; another set of experiment was set up with the following parameters: TR: 100, 200, 500, 1000, 2000, 5000 ms TE:11 ms, number of acquisitions: 3. T_2 and T_1 weighted images intensities (I) was used for the calculation of T_2 and T_1 values using the curve fitting toolbox of Matlab using the following formula;

$$T_r \gg T_1 \qquad I \; \alpha \; e^{-T_E/T_2} \qquad 1.5$$

$$T_E \ll T_2 \qquad I \; \alpha \; e^{-T_1/T_R} \qquad 1.6$$

The r_1 and r_2 values were calculated based on the relaxation rate versus iron concentration determined with Prussian blue colorimetric assay.

CHAPTER 3

RESULTS AND DISCUSSIONS

3.1. Synthesis of SPIONs

According to the chemical route, synthesis of iron oxide nanoparticles can be classified in two categories which are hydrolytic and non-hydrolytic. The hydrolytic synthesis routes, such as co-precipitation rely on hydrolysis of ferric and ferrous ions, while non-hydrolytic routes, such as thermal decomposition, rely on pyrolysis of iron-organic compounds. Herein, we performed and compared both co-precipitation and thermal decomposition methods for the synthesis of SPIONs and results were discussed by means of the particle size, shape and monodispersity [19].

3.1.1. Synthesis of SPIONs via Co-Precipitation Method

The co-precipitation method is the most widely used method which has been firstly reported by Welo et al. who produced magnetic particles in 1925[5]. Many methods were developed later on. Basic principles in magnetite formation can be explained by Lewis acid-base concepts. The iron atom on the SPION surface is a hard Lewis acid, while compounds which are able to accept oxygen atom (O^-), water or NH_3, are hard lewis bases. Therefore,

based on this theory, hard acids are able to react faster and form strong bonds with hard bases as stated in Lamer diagram above [22].

For the SPION synthesis via co-precipitation method, iron (II) chloride and iron (III) chloride were mixed in 2:1 molar ratio at low pH around 2 to 3. 1 M ammonium hydroxide solution was deoxygenated with nitrogen gas. Further, pH of the ammonium hydroxide solution was adjusted to pH 11 and iron solution was quickly poured into the ammonia solution under continues sonication. They were sonicated for 30 min under nitrogen gas. Resulting particles were analyzed by FT-IR and DLS and SEM at this step. According to results from SEM shown in Figure 7, particles tend to aggregate into larger particles with size range that is not suitable for their use in medicine.

Particle surface properties and their crystalline state were characterized by FT-IR. Obtained peak at 577 cm^{-1} in Figure 7 belongs to Fe-O stretching band which represents the existence of magnetite crystals[23]. At this step, SPIONs surface were coated with MTBS. It would not only to avoid the particle aggregation but also to functionalize them. MTBS has two carboxyl groups and one of those carboxyl groups was modified with a protective group. When MTBS treated with highly acidic or basic solution, the protective group detached. After the attachment of MTBS to the SPION, solution was treated with basic solution. To detect free carboxyl group on SPION surface, FT-IR was analysis were pursued. As reported earlier in the literature, free carboxyl group peak locates at 1400 cm^{-1} which was not

present in our FT-IR results in Figure 9. According to these results, SPION surface modification with MTBS was not successful.

SPION size after the MTBS modification were measured with DLS and visualized through the SEM. According to results presented in Figure 10, the hydrodynamic size of the particles was around 65 nm which is highly correlated with SEM results.

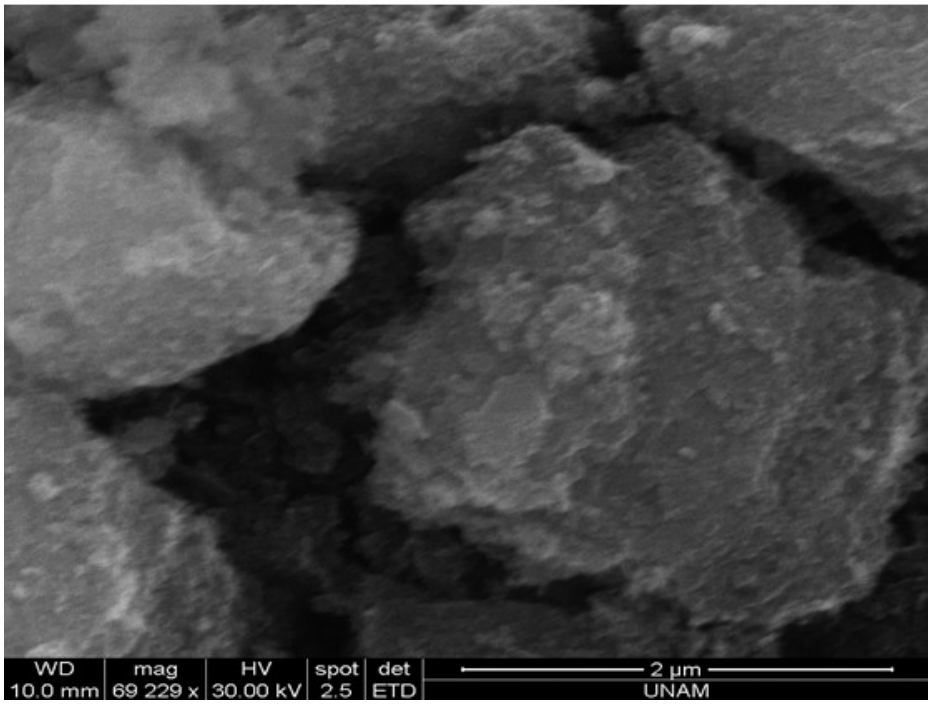

Figure 7. SEM image representing the large aggregations ofSPIONs when they synthesized with co-precipitation method.

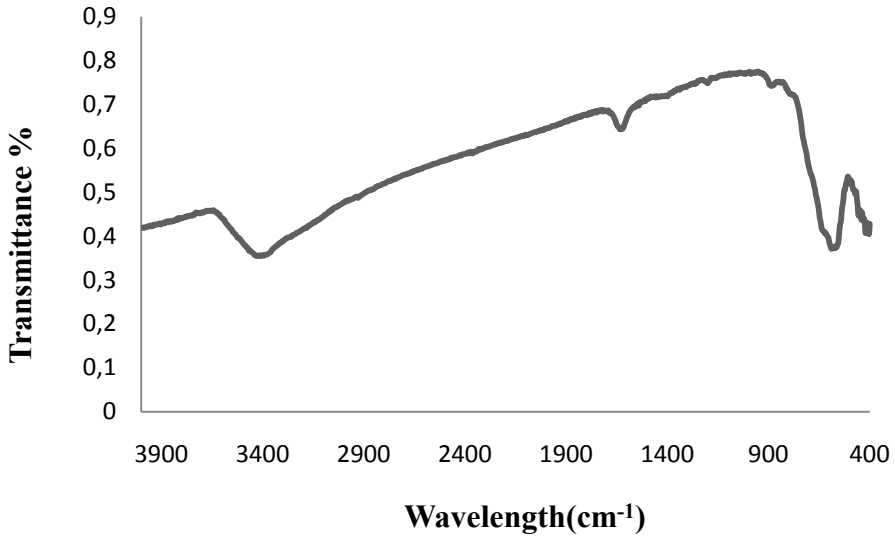

Figure 8. The FT-IR spectrum of SPIONs synthesized by co-precipitation method. The existence of Fe-O strecting peak at 570 cm^{-1} proves that particles were at magnetite phase.

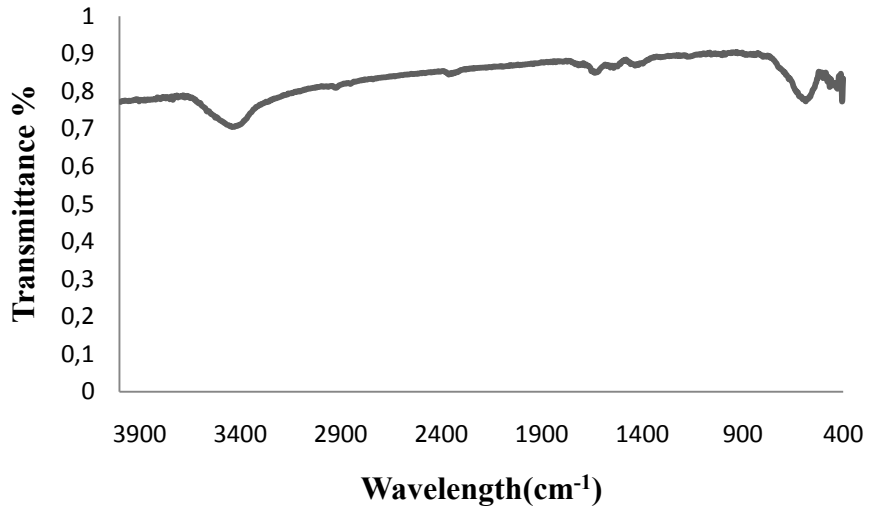

Figure 9. The FT-IR graphic of mono tert-butyl succinate functionalized SPIONs. There is no carboxyl peak around 1400 cm^{-1} which means that surface modification was not successful.

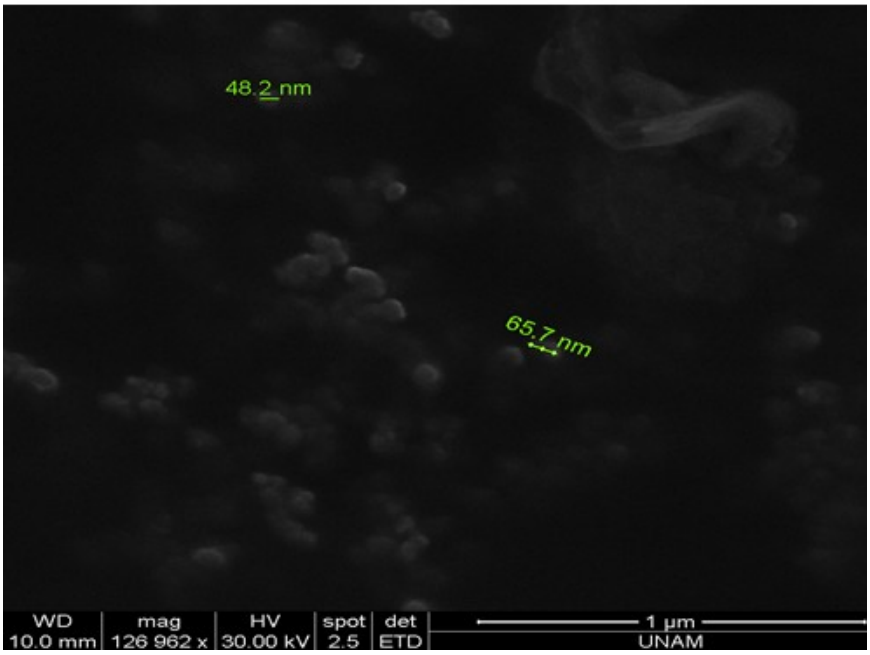

Figure 10. SEM images of MTBS modified SPIONs synthesized by co-precipitation method. Particles were still aggregated after MTBS treatment.

Co-precipitation is an easy technique to synthesize SPIONs. However, it is rather complex technique since the particle characteristic (shape, size and its distribution, and crystal phase) are affected by many factors such as pH, concentrations of iron salts, ratio of Fe^{2+}/Fe^{3+} [19]. As a result of these, poly-dispersity of the SPION population prepared via co-precipitation method is high (Figure 7). Also, surface modification on SPIONs is much harder than the other nanoparticles, such as gold nanoparticles, due to their surface properties and necessity of the non-oxidized environment during the modification.

3.1.2 Synthesis of SPIONs with Thermal Decomposition Method

Among the non-hydrolytic synthetic routes, thermal decomposition based on the pyrolysis of the organometallic compounds has become the most widely used and successful approach to synthesize SPIONs with perfect monodispersity, size tunability, high crystallinity [19]. Alivisatos et al. was the first group who synthesized maghemite nanoparticles with thermal decomposition method, however, method reported by Sun et al. is the most widely used and accepted method for SPION synthesis using thermal decomposition method [10,19].

Although the exact mechanism behind the thermal decomposition method is still vague, experimental parameters reveal some important features. High-temperature reaction of $Fe(acac)_3$ with polyols, lauric acid, and dodecylamine in high boiling ether solution allowed the formation of nanosized magnetite with well controlled size and size distribution with high crystallinity [7,11,19,23]. Polyols are used as a chelating agent, which have high dielectric constant and high donor number where these polyols forms stronger associates with metal ions[19]. Lauric acid and dodecylamine are used as stabilizing agents to control size of the SPIONs and inhibit the aggregation during the synthesis. High boiling ether solution is used as solvent and it determines the size fate of the nanoparticles. The key for the efficient synthesis of SPIONs relies on preheating step where the reaction solution is heated up to 200 ºC. This step is highly effective on the size

distribution of the nanoparticles [10]. Although the exact mechanism is not known, researchers hypothesize that at preheating step acetylacetonate group of $Fe(acac)_3$ exchanges with the polyols added into the solution [3]. The crystal phase of the SPIONs is determined by the reflux step. Refluxing time has to be optimized to be able to get SPIONs in magnetite phase; in low refluxing time, it was shown that non-magnetic Fe-O could be synthesized [7].

By thermal decomposition method developed by Sun et al., we were able to synthesize monodisperse uniform nanoparticles with diameters of 6-7 nm as represented in Figure 11. Lauric acid and dodecylamine were used as surfactant. The carboxyl and amine head groups were attached to the SPION surface during the synthesis and tailed away. End product is soluble in organic solvent. The core of the SPIONs was characterized with XPS and XRD methods. According to obtained results in Figure 12 IOPs are in magnetite phase [10] which have the highest magnetization value. The magnetization value represents the response of materials to the magnetic field. and their magnetization saturation was 56 emu/g (Figure 13). Moreover, hysteresis loop also showed that the nanoparticles were superparamagnetic.

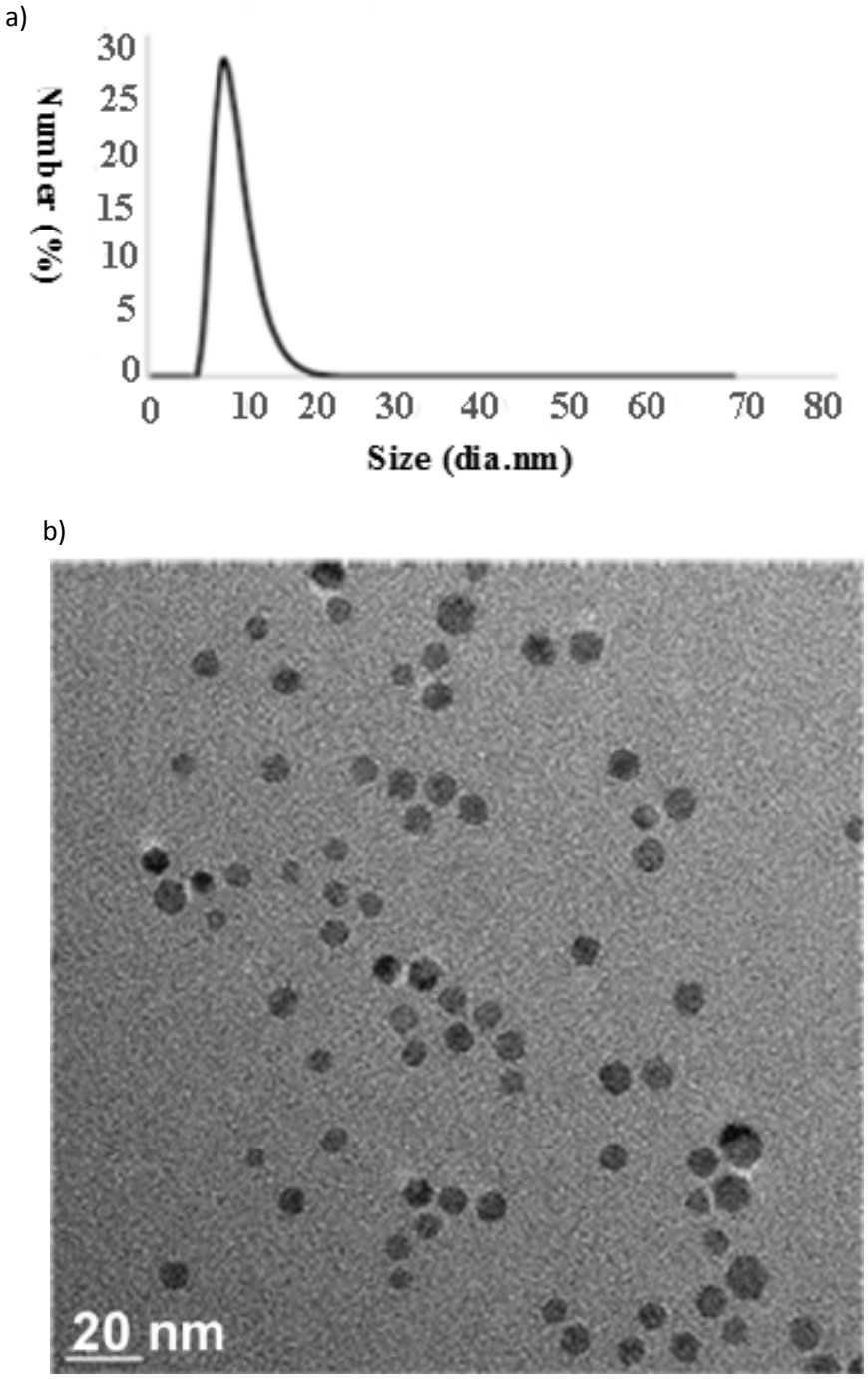

Figure 11. Characteristics of SPIONS synthesized via thermal decomposition method: **a)** Hydrodynamic size of the SPIONs, **b)** TEM images illustrating the monodisperse SPIONs of around 7 nm.

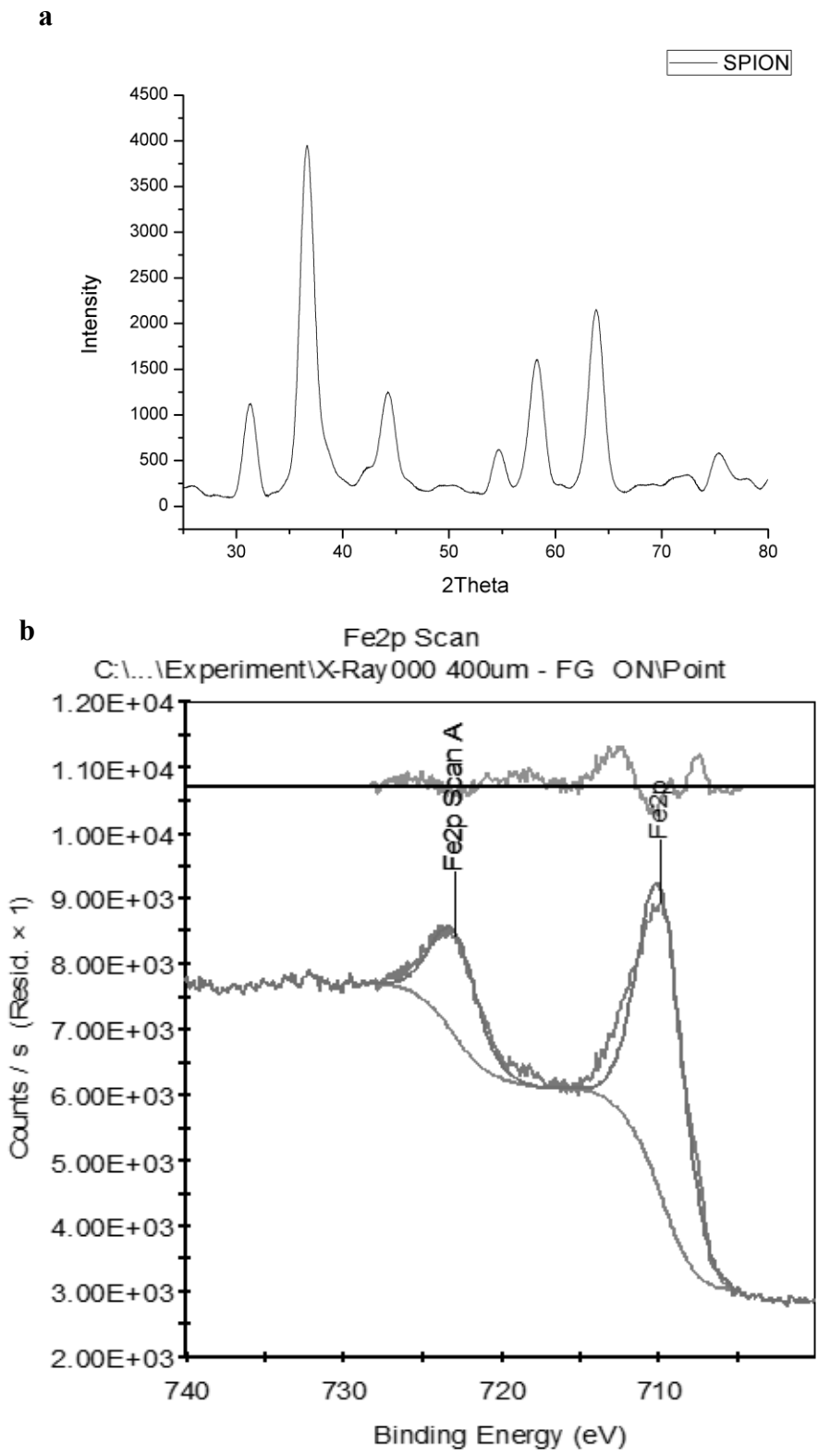

Figure 12. a) XRD spectrum graphic and **b)** XPS spectrum of SPIONs synthesized with thermal decomposition method showing that produced particles are in magnetite phase.

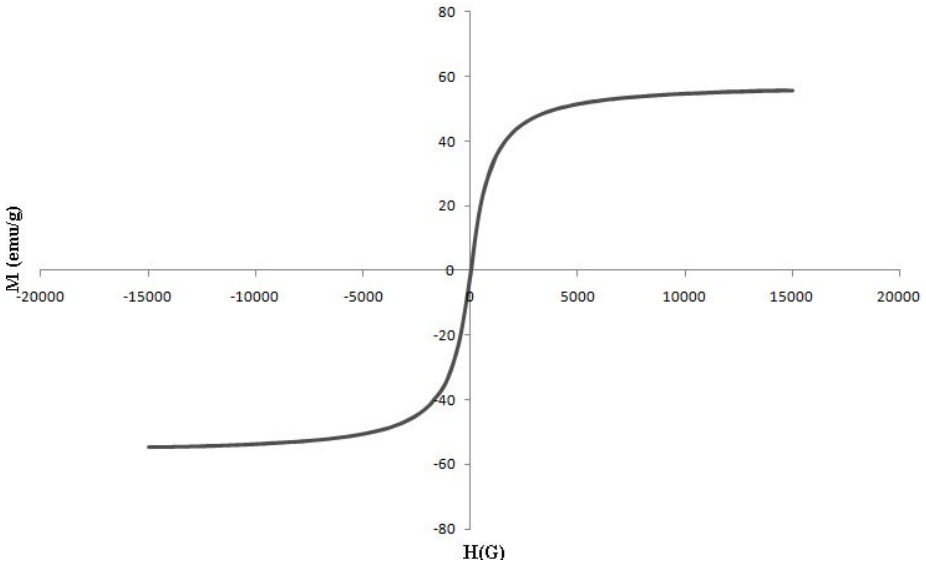

Figure 13. Hysterysis loop of SPIONs synthesized with thermal decomposition method. The hysterysis revealed that particles were represents superparamagnetic behaviour and their magnetization value was 56 emu/g.

3.2. Peptide Amphiphiles

Solid phase peptide synthesis protocol was used for the synthesis [4]. The process was briefly represented in Figure 14. Deblocking, activation, coupling, as well as cleavage and deprotection are the critical steps in the peptide synthesis. In SPPS protocol peptide is constructed on an insoluble solid support since the separation of the peptide from soluble reagents and the removal of excess reagents could be much easier if resin support is used. In deblocking step, the protecting group on the amino acid will be removed. 9-fluorenylmethoxycarbonyl (Fmoc) is one of the protecting groups, and it has been employed in this study to protect the N- terminus. It is a base-labile protecting group and piperidine can be used for deblocking of the aminoacid. The fmoc group localized on resin was removed firstly and the first activated aminoacid was added. For the aminoacid activation several

methods exist in the literature and HBTU/DIEA activation method was used to activate carboxyl group of amino acids in this study, then the amino acid can easily couple with resin and/or amino acid. Deprotection of the Fmoc Group from the first amino acid and second amino acid was coupled, and this procedure repeated until a desired peptide obtained. After each coupling step, resin was washed with acetic acid to deactivate free amine group. This step is necessary to improve the purity. In the final step, peptide was deprotected and TFA cleavage was done to detach the peptide from the resin [4].

For the encapsulation of SPIONs, amphiphilic peptides were used. The lauric acid adds the hydrophobic character to peptide amphiphiles, whereas aminoacid sequences supply hydrophilic and biofunctional feature. The chosen peptide molecules were **PA-1** (Lauryl-VVAGK) (depicted as 1 in Figure 15), **PA-2** (Lauryl-VVAAD-Am) (depicted as 2 in Figure 15), **Pro-PA(1)** (Lauryl-PPPE) (depicted as 4 in Figure 15), **Pro-PA(2)** (Lauryl-PPPPGE) (depicted as 1 in Figure 15). **PA-1** is positively charged molecule at neutral pH whilst the **PA-2** is a negatively charged molecule at neutral pH. These peptides can form self-assembled structures. They have no specific response to any tissue or cell; they have self-assemble and have charge feature. Herein, we want to monitor the effect of charged peptides on the synthesis of the SPIONs and also the effect of produces SPIONs on living cells. **Pro-PA(1)** and **Pro-PA(2)** are negatively charged peptides. The proline aminoacid is districted to the existence of hydrogen bonds, so it cannot form self- assembled structures. These peptides were selected for the

protein conjugation studies. The mass spectrometry and the HPLC chromatograms can be seen in Figures 16-23. We faced serious problems in the synthesis of the **Pro-PA(1).** Based on these serious problems, an alternative peptide, **Pro-PA(2)** was synthesized.

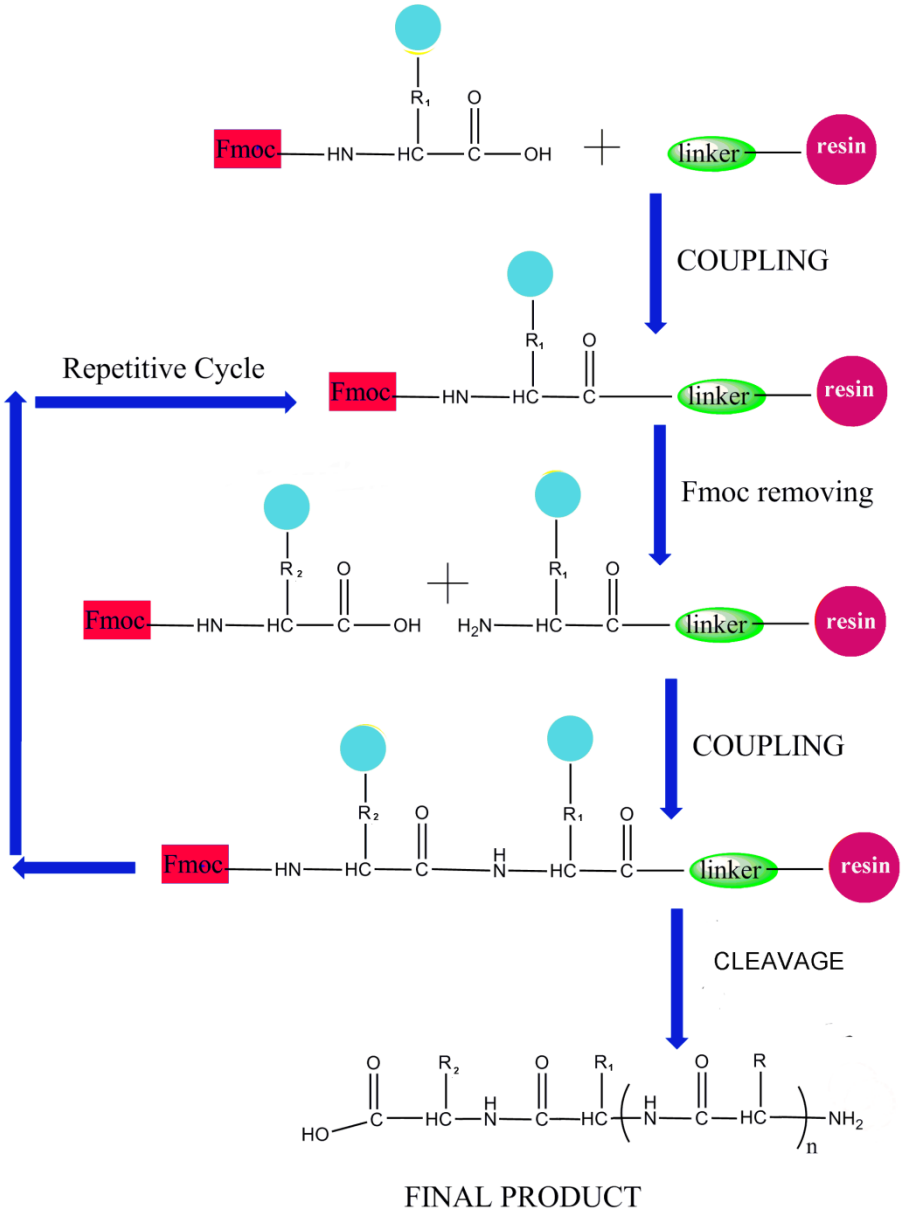

Figure 14. A schematic representation of solid phase peptide synthesis. The protected aminoacid was activated from its carboxyl group. Then it was coupled to the other aminoacid from its amine reactive group. After the final deblock peptide was cleaved from resin.

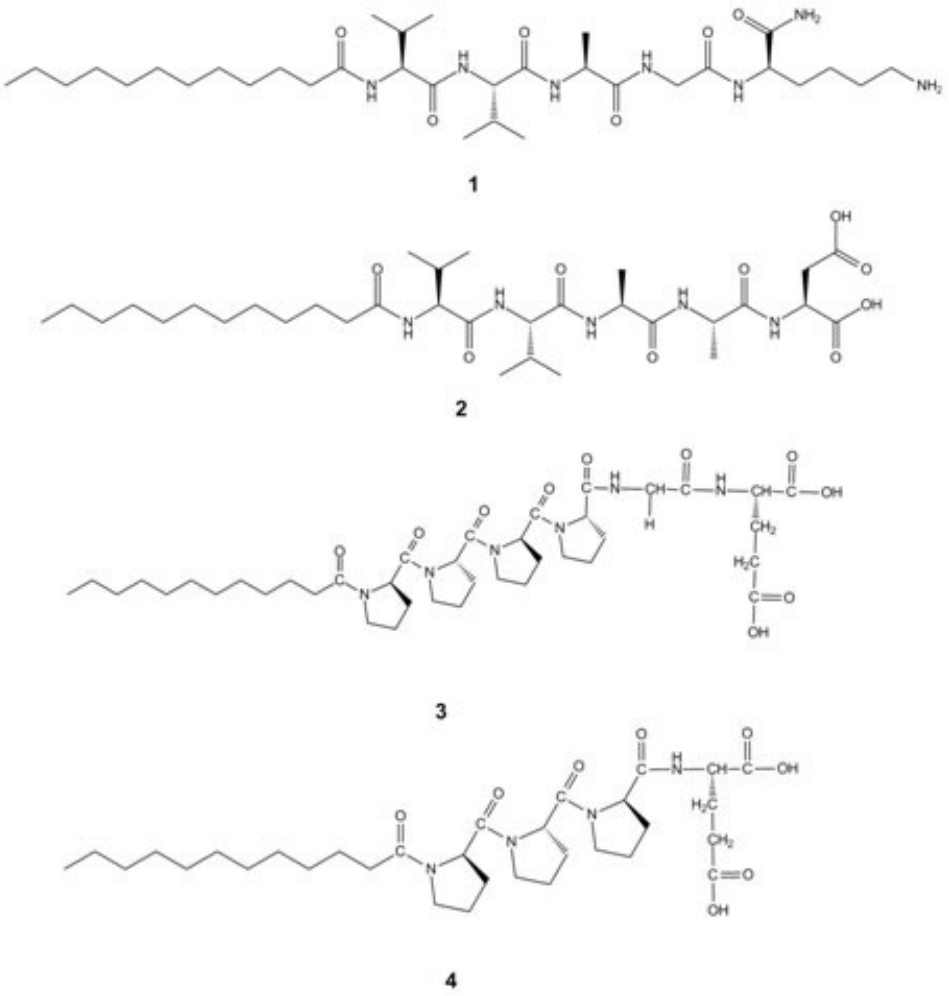

Figure 15. Chemical representation of PAs used for surface modification of SPIONs in order to increase their solubility in water and biocompatibility: **1)** amide functionalized PA-1, **2)** carboxylic acid functionalized PA-2; and carboxylic acid functionalized **3)** Pro-PA(2) and **4)** Pro-PA(1) which do not form hydrogen bond because of proline sequences.

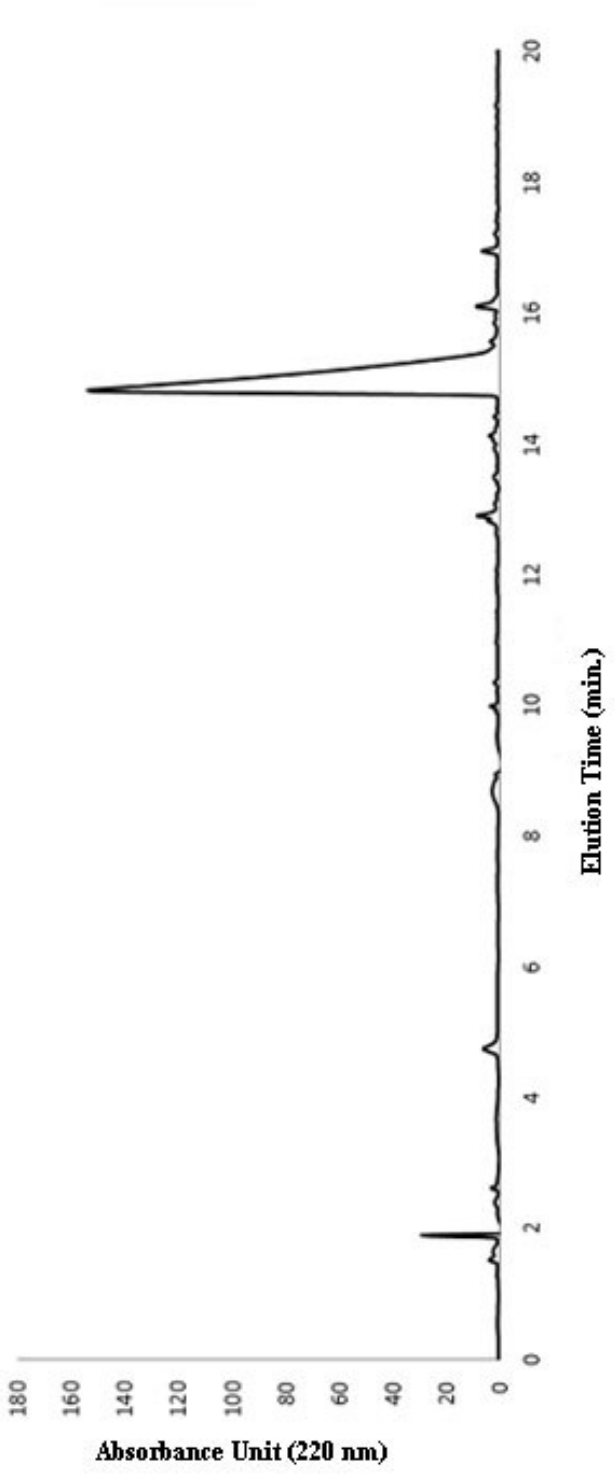

Figure 16. RP-HPLC chromatogram of PA-1. Absorbance at 220 nm vs. retention time graph. HPLC results revealed that the synthesized peptides were more pure than 90%.

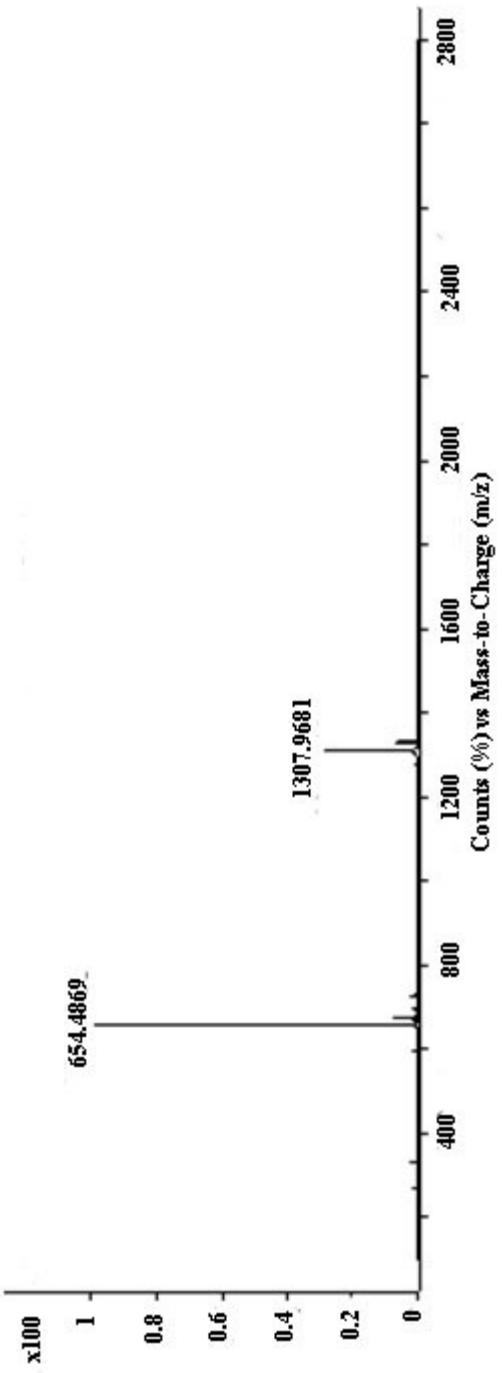

Figure 17. Mass spectrometry of the PA-1. $[M+H]^+$ (calculated)=654.48 $[M+H]^+$ (observed)=654.49, $[2M+H]^+$ (calculated)=1307.96 $[2M+H]^+$ (observed)=1307.96. Theoretical and experimental values were matched with each other.

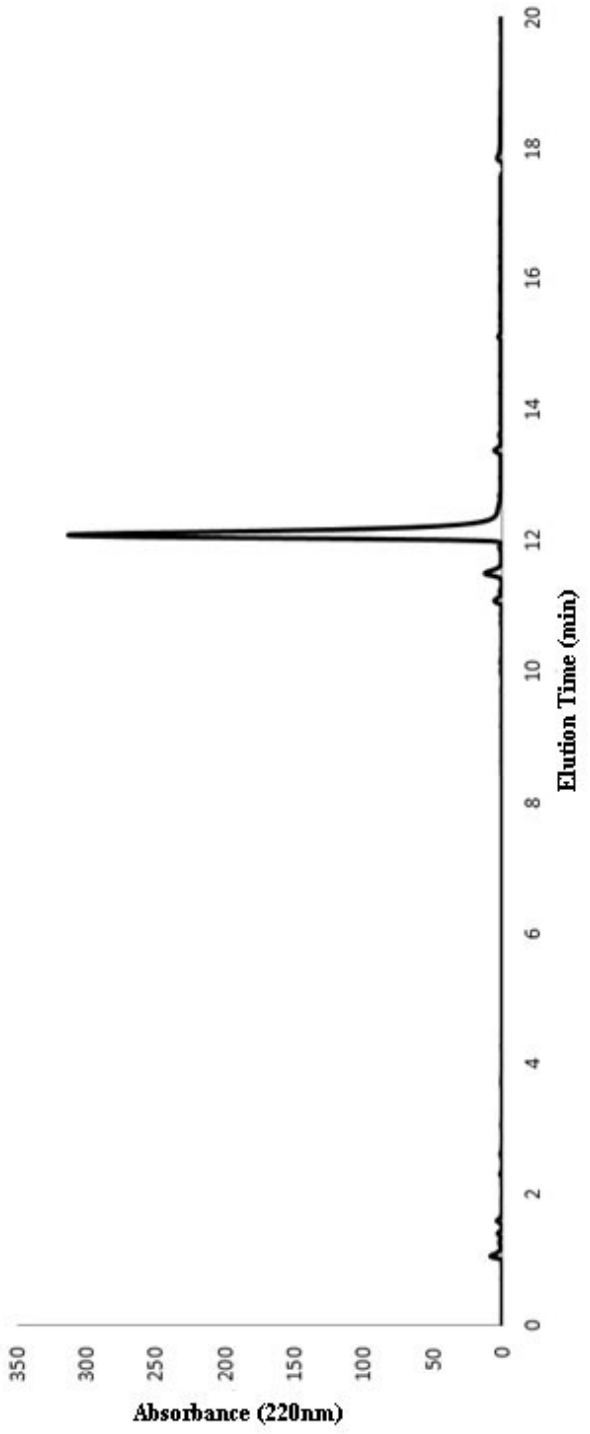

Figure 18. RP-HPLC chromatogram of PA-2. Absorbance at 220 nm vs. retention time graph. HPLC results revealed that the synthesized peptides were more pure than 90%.

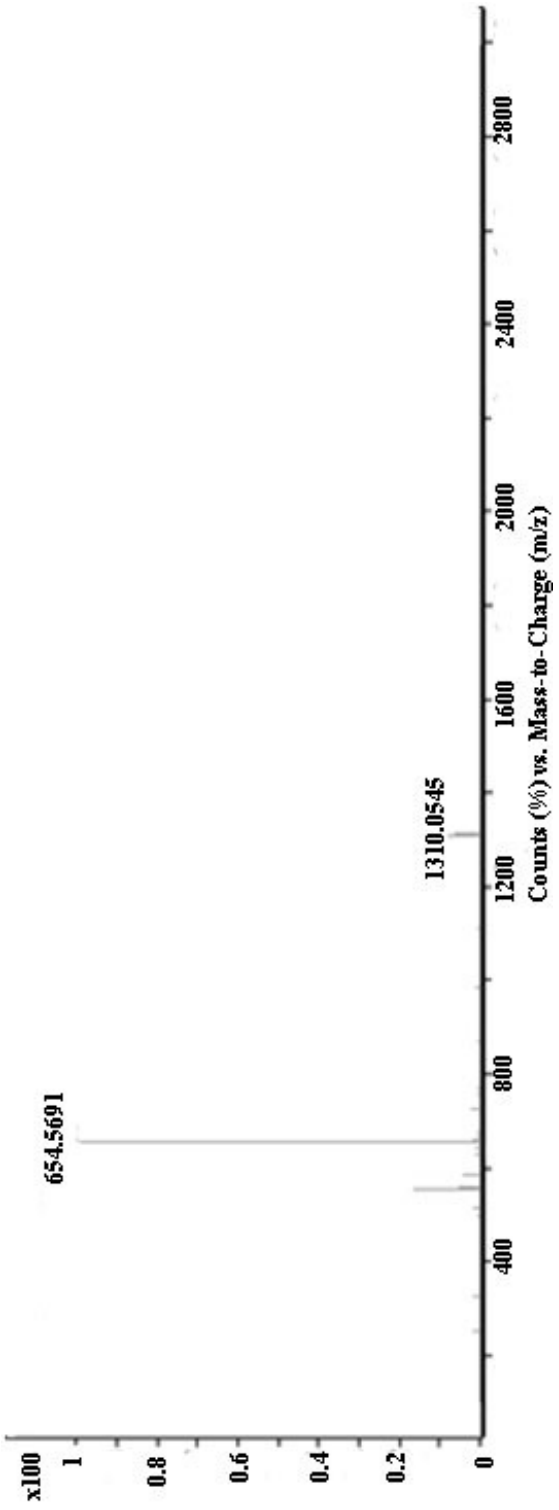

Figure 19. Mass spectrometry of PA-2. $[M-H]^+$ (calculated)=654.56 $[M-H]^+$ (observed)=654.56, $[2M-H]^+$ (calculated)=1310.05 $[2M-H]^+$ (observed)=1307.05. Theoretical and experimental values were matched with each other.

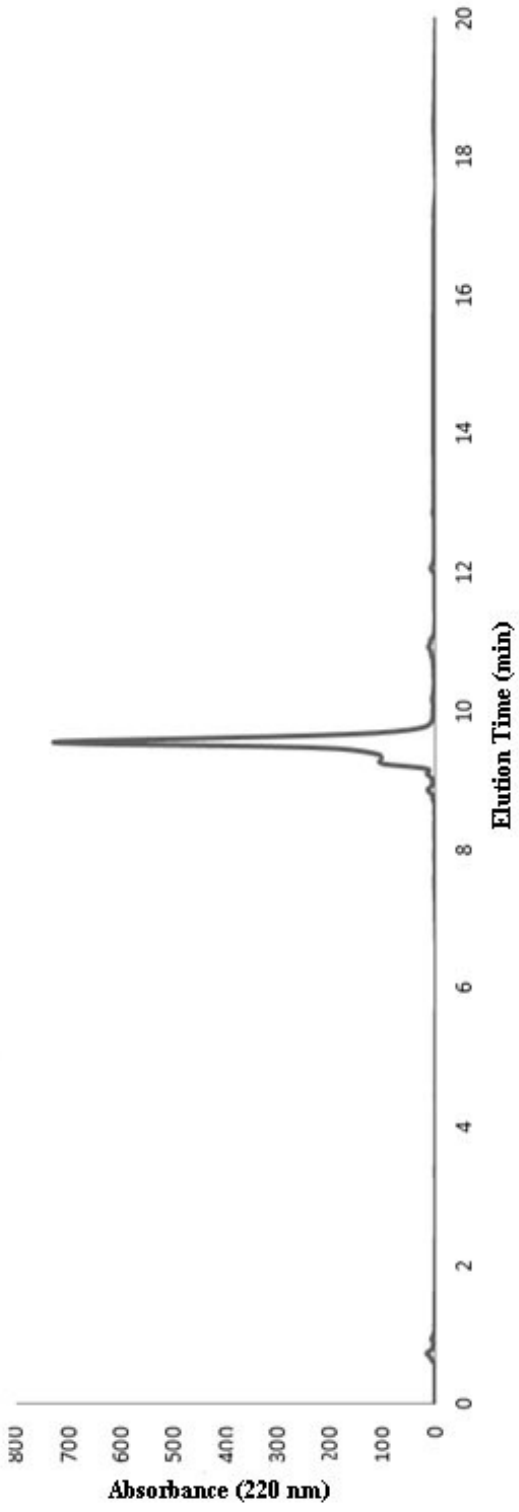

Figure 20. RP-HPLC chromatogram of Pro-PA(2). Absorbance at 220 nm vs retention time graph. HPLC results revealed that the synthesized peptides were more pure than 90%.

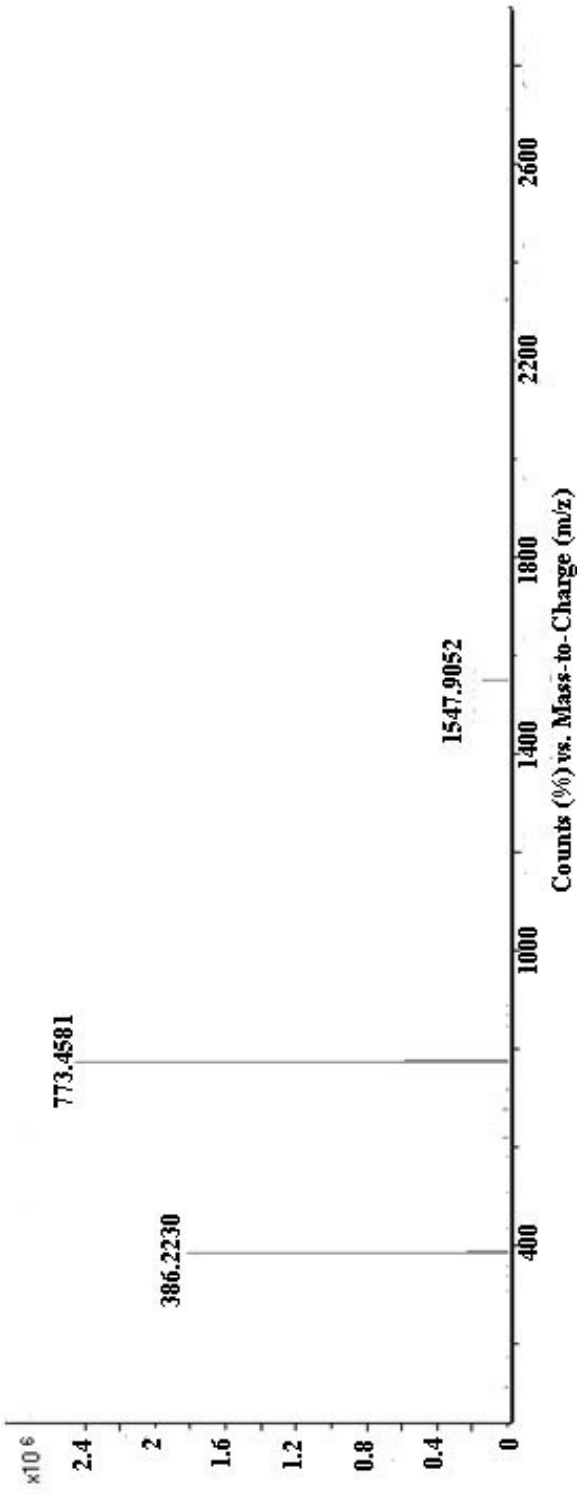

Figure 21. Mass spectrometry of Pro-PA(2). $[M-H]^+$ (calculated)=773.45 $[M-H]^+$ (observed)= 773,45 , $[2M-H]^+$ (calculated)=1547.9 $[2M-H]^+$ (observed)=1549.9, $[M/2-H]^+$ (calculated)=386.2 $[M/2-H]^+$ (observed)=386.2. Theoretical and experimental values were matched with each other.

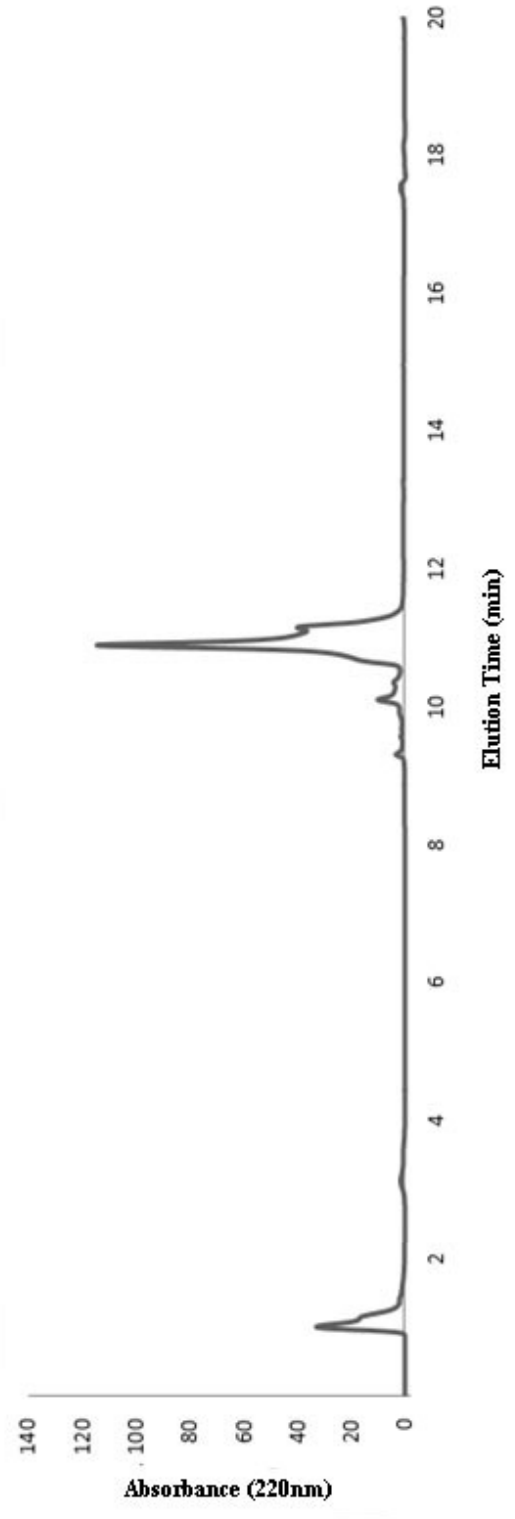

Figure 22. RP-HPLC chromatogram of Pro-PA(1). Absorbance at 220 nm vs retention time graph.

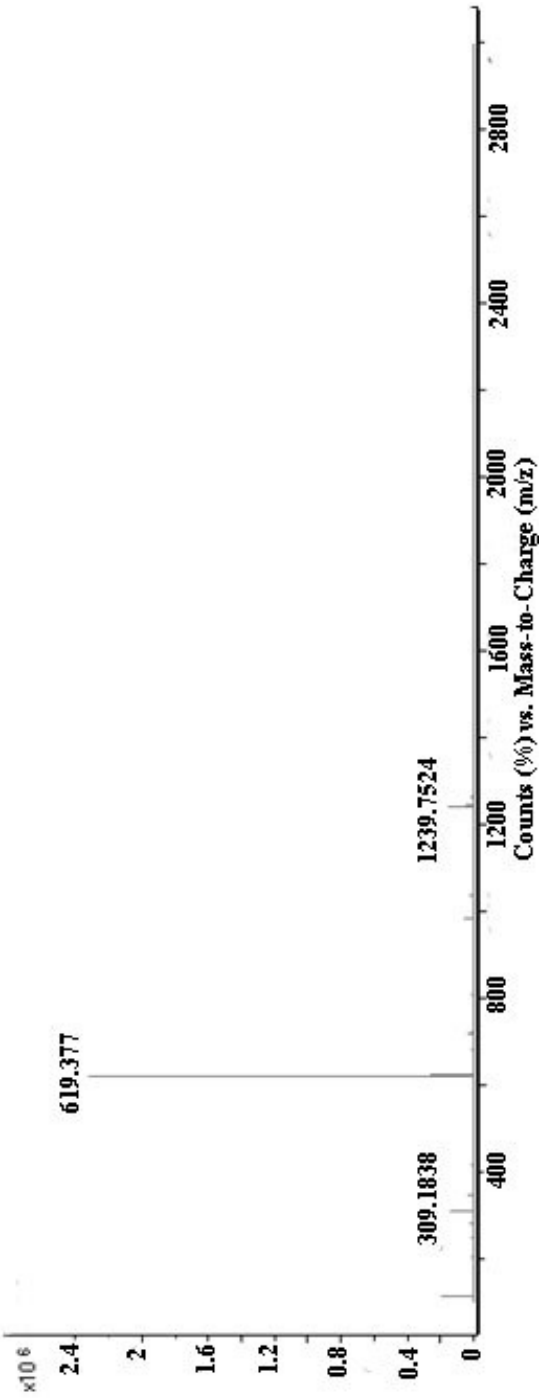

Figure 23. Mass spectrometry of Pro-PA_1. $[M-H]^+$ (calculated)=619,37 $[M-H]^+$ (observed)= 619,37 , $[2M-H]^+$ (calculated)=1239.75 $[2M-H]^+$ (observed)=1239.75, $[M/2-H]^+$ (calculated)=309.18 $[M/2-H]^+$ (observed)=309.18. Theoretical and experimental values were matched with each other.

3. 3. Synthesis of Peptide-SPION Complex and Their Physicochemical Properties

Surface group of the SPION has to meet three features: (i) binding region, (ii) water soluble region and (iii) bioactive region [7]. There are numerous attempts to meet these three features [11]. Herein, we developed a novel method to functionalize SPIONs for medical use by exploiting the peptide amphiphiles for surface functionalization.

SPIONs were synthesized with thermal decomposition method and lauric acid was used as surfactant to coat SPION surfaces. The end products are stable in organic solvents because of the carboxyl group of lauric acid which bounded hydrophobic region tailed away. Lauryl group of the peptide amphiphiles interacts with the alkyl groups located on SPIONs hydrophobically, and not only forms stable nanoparticles in aqueous solutions but also provides bioactivity since PAs can be modified by various peptide sequences for targeting to desired type of cell and/or molecule. A representative Figure is presented in Figure 24.

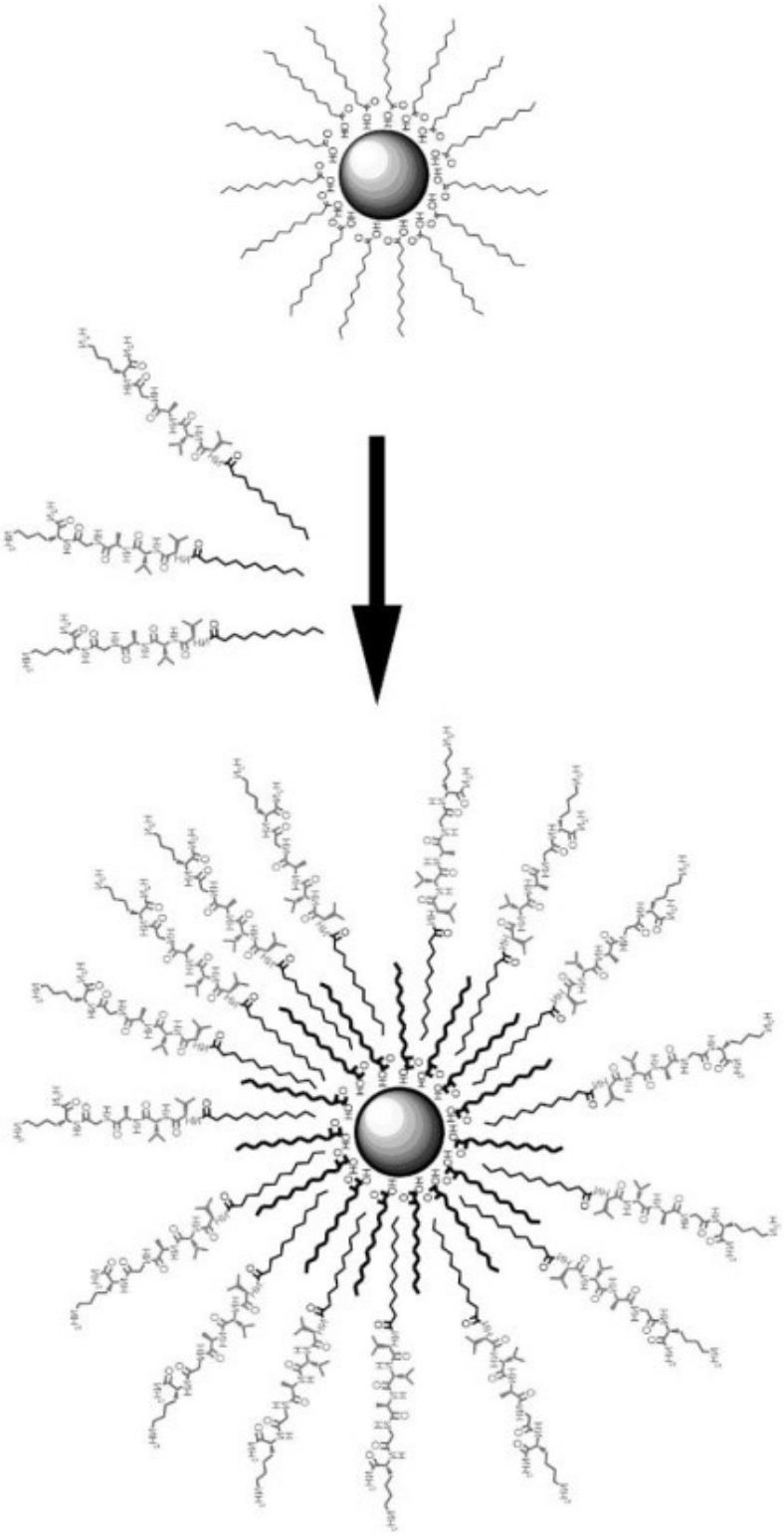

Figure 24. Non-covalent functionalization of SPIONs with peptide amphiphile molecules. Hydrophobic part of PA and magnetite intercalate with each other in aqueous solvent.

Synthesis procedure of peptide-SPION complex was optimized and it was found to be 7 mg PA to 1 mg SPION and the optimum volume for the mixture was 10 ml PA solution in water to 1 ml SPIONs in hexane. Excess amount of PA was used at the optimum volume to prevent aggregation of SPIONs. Aggregated SPIONs were removed by 0.2 μm cut-off filter and excess PA was dialyzed with 500-1000 Dalton cellulose membrane bags. After the PA coating phase transition occurred, SPIONs were transferred to water from organic solvent (Figure 25 a,c,e). FT-IR spectrum in Figure 27 revealed the existence of amine and amide peaks due to the presence of peptide on the SPION surface. TEM characterization of SPIONs revealed that SPIONs had narrow size distribution even after PA coating, and are stable in aqueous solution (25-40 nm in diameter) (table 1, Figure 25 and Figure 26) XRD pattern shown in Figure 2g demonstrates that SPIONs stayed still in magnetite form similar to the unmodified ones.

The magnetic properties of the SPIONs were examined with VSM. The saturation magnetization (M_s) of lauric acid stabilized SPION was found to be 56 emu g^{-1}. After functionalization process, peptide coated SPIONs M_s dramatically decrease to 5 emu g^{-1} and 8 emu.g^{-1} for **PA1-SPION** and **PA2-SPION,** respectively, (Figure 28) the decrease in M_s value was caused by the peptide coating[24]. Moreover, as shown in Figure 28, peptide-SPION complexes have zero coercivity fields indicating that these nanoparticles are superparamagnetic.

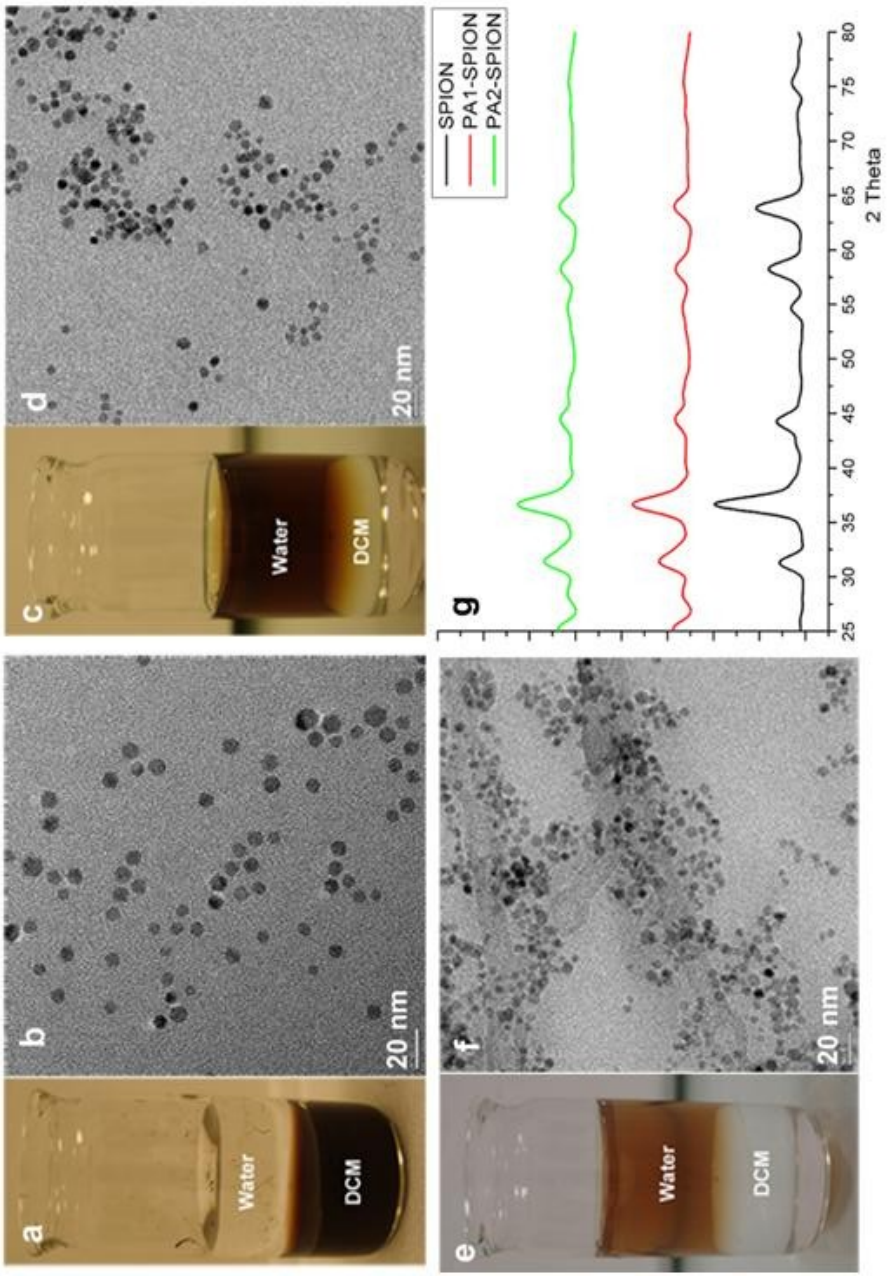

Figure 25. Dichloromethane **(**DCM)-water phase image of lauric acid coated SPIONs **b)** TEM image of lauric acid coated SPION **c)** DCM-water phase image of **PA1**-SPION complex **d)** TEM image of **PA1**-SPION complex **e)** DCM-water phase image of **PA2**-SPION **f)** TEM image of **PA2**-SPION **g)** XRD pattern of lauric acid coated SPION, **PA1**-SPION and **PA2**-SPION. Images at a,c,e reveal that phase transition was successful. TEM pictures show that particles were stable in aqueous solvent. According to XRD results, the core complexes were not changed after the encapsulation and remain in magnetite phase.

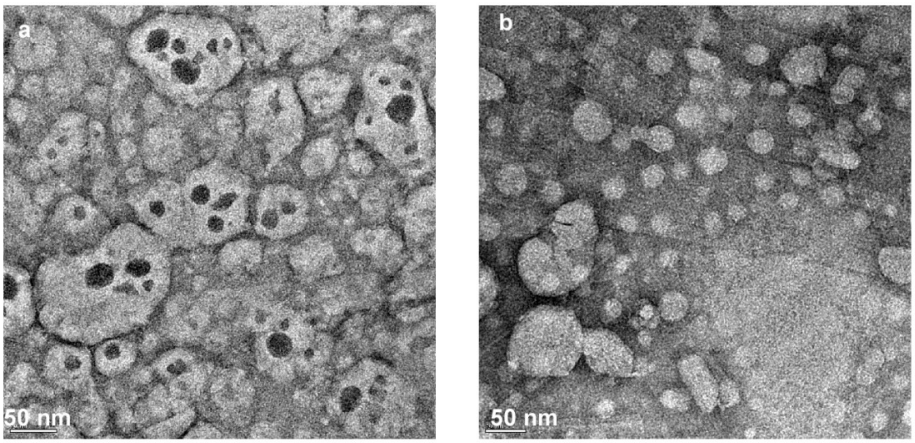

Figure 26. TEM image of **PA1**-SPION complex stained with uranyl acetate. **b)** TEM image of **PA2**-SPION complex stained with phosphotungstic acid. Uranyl acetate is able to bind organic molecules whereas phospotungstic acid dyed the background. Based on the stained particles and background, the encapsulated particles total sizes were around 30 nm.

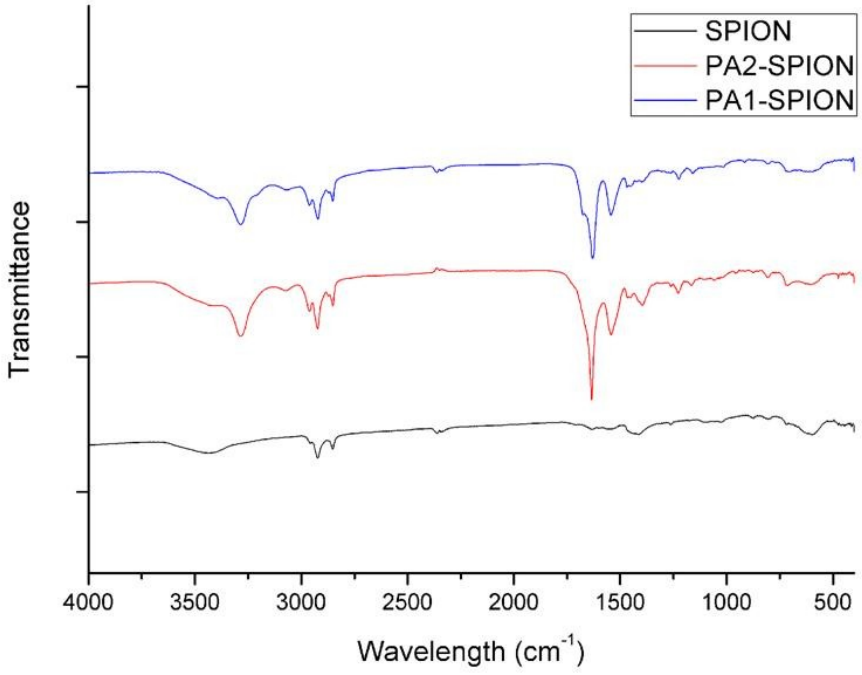

Figure 27. FT-IR spectra of SPION, **PA1**-SPION and **PA2**-SPION. The lauric acid located on SPION surface did not contain amide group. However after the encapsulation, peaks around 1560 cm^{-1} and 3300 cm^{-1} were observed demostrating the existence of PA around the magnetic nanoparticles.

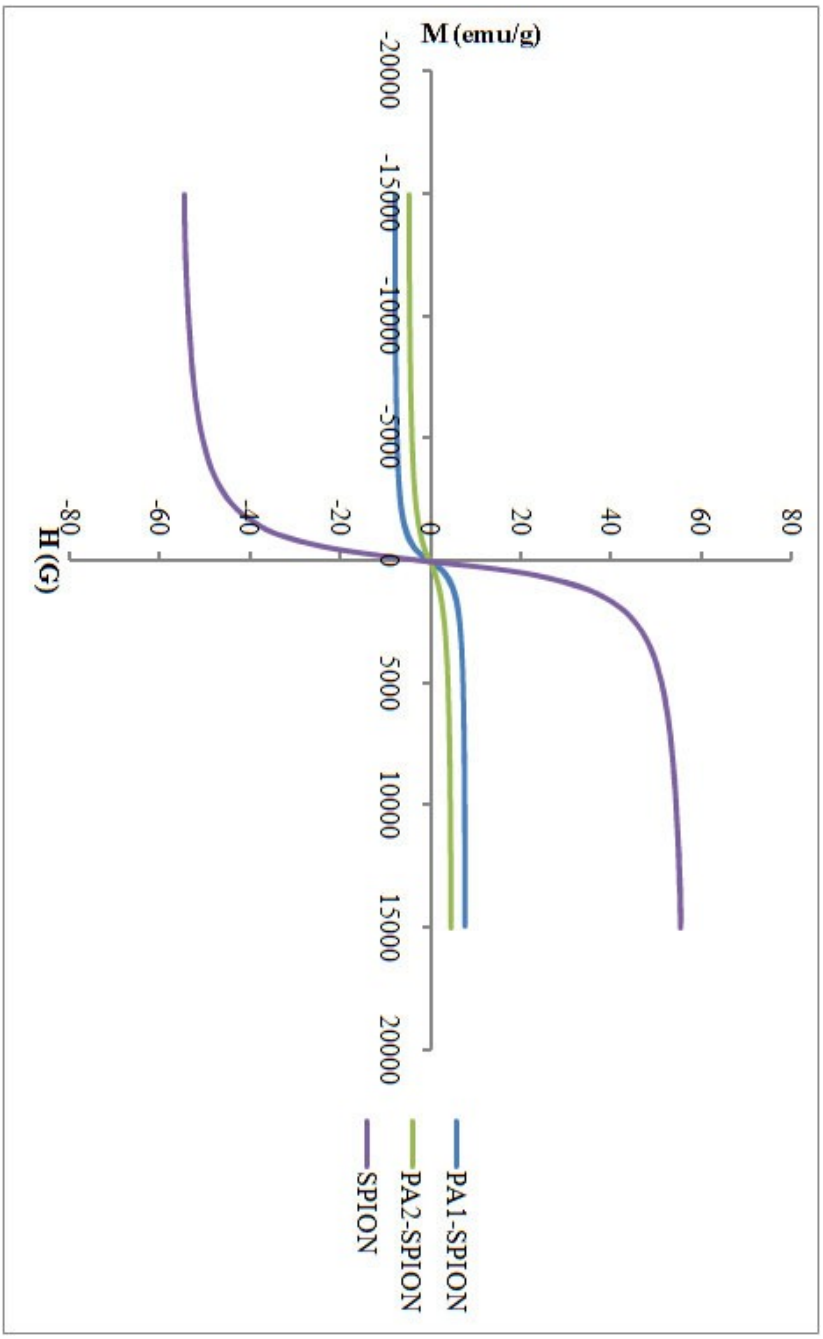

Figure 28. Hysteresis loop graphs of **PA1**-SPION, **PA2**-SPION and SPION obtained by VSM. Although, their magnetization value decreased, particles still presents superparamagnetic behavior after PA modification.

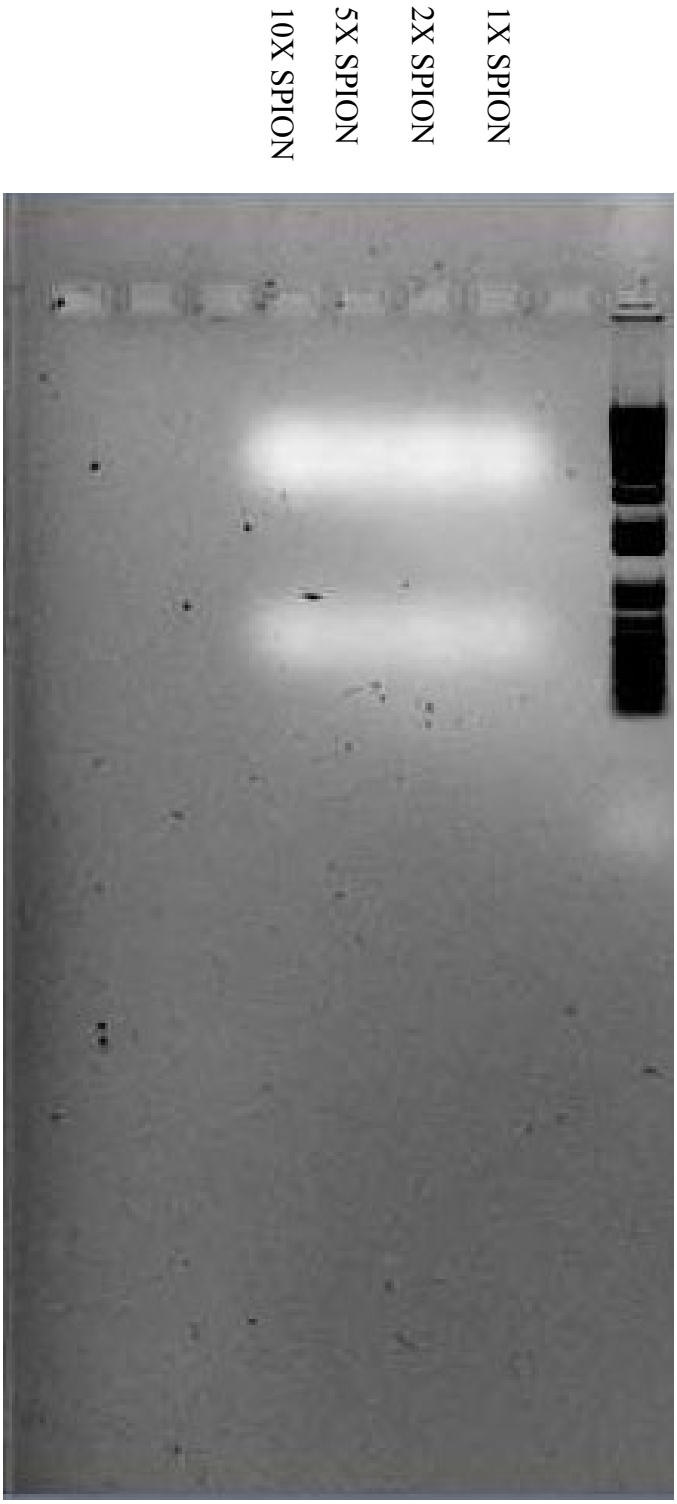

Figure 29. Gel Electrophoresis Results of Pro-PA(2) functionalized SPIONs. PA-SPION complexes cannot be observed after encapsulation since particles were not stable in electrical field and decomposed when electrical field applied.

To analyze the purity of the SPION population obtained, gel electrophoresis was applied to the sample with 1X TAE buffer at 120V for an hour. According to the gel electrophoresis result shown in Figure 29, peptide-SPION complex was affected by electrical field and decomposed. Then the purity of the peptide-SPION complex was studied with UV Nano-drop. Peptides have a specific absorbance at 205 nm[25]. Peptide concentration was calculated based on the absorbance value at 205 nm wavelength (extinction coefficient chosen as 31) [25]. To remove the excess amount of peptide, the solution was firstly centrifuged at 12500 rpm for 15 min. Then it was centrifuged at 10000 rpm for 15 min. According to the UV spectrophotometry measurements, peptide concentration was found to be 4.97 mg/ml before the washing step, and 0.198 mg/ml after (Figure30).

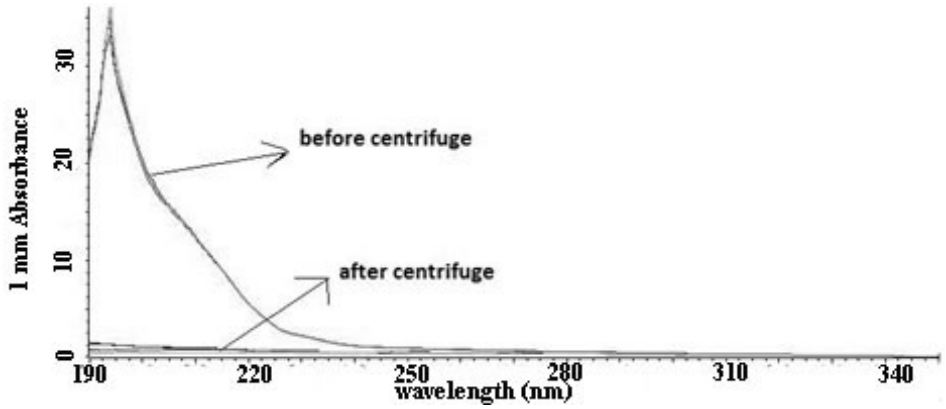

Figure 30. UV spectrum of peptide-SPION solutions before and after washing step. Excess peptides were successfully removed after 2 subsequent centrifugation steps.

Contrast agents locally enhance the response of the water molecules to the magnetic field[15]. SPIONs are negative contrast agents and they reduce T_2 relaxation time of the water protons resulting in darker signals, and the efficiency of the contrast agent depends on the relaxivity and r_2/r_1 values[26]. Relaxation rates R1 and R2 reveal the relaxivity values r1 and r2 of SPIONs which depend on the total metal concentration. These values were investigated under 3T magnetic field and r_1 and r_2 relaxivity values of PA1-SPION and PA2-SPION were measured. r_1 and r_2 values of PA1-SPIONs were 0.9 $mM^{-1}s^{-1}$ and 100.4 $mM^{-1}s^{-1}$, whereas, that of PA2-SPION were 1.8 $mM^{-1}s^{-1}$ and 93.7 $mM^{-1}s^{-1}$, respectively (Figure 31, table 1). As mentioned above, r_2/r_1 is another feature determining the efficiency of the SPIONs. Measured value of r_2/r_1 ratio for **PA1**-SPION was 111.55 and 52.1 for **PA2**-SPION. The r_2 values observed here were close to the commercial ones, whereas r_2/r_1 values were much greater than the commercial ones [27-30].

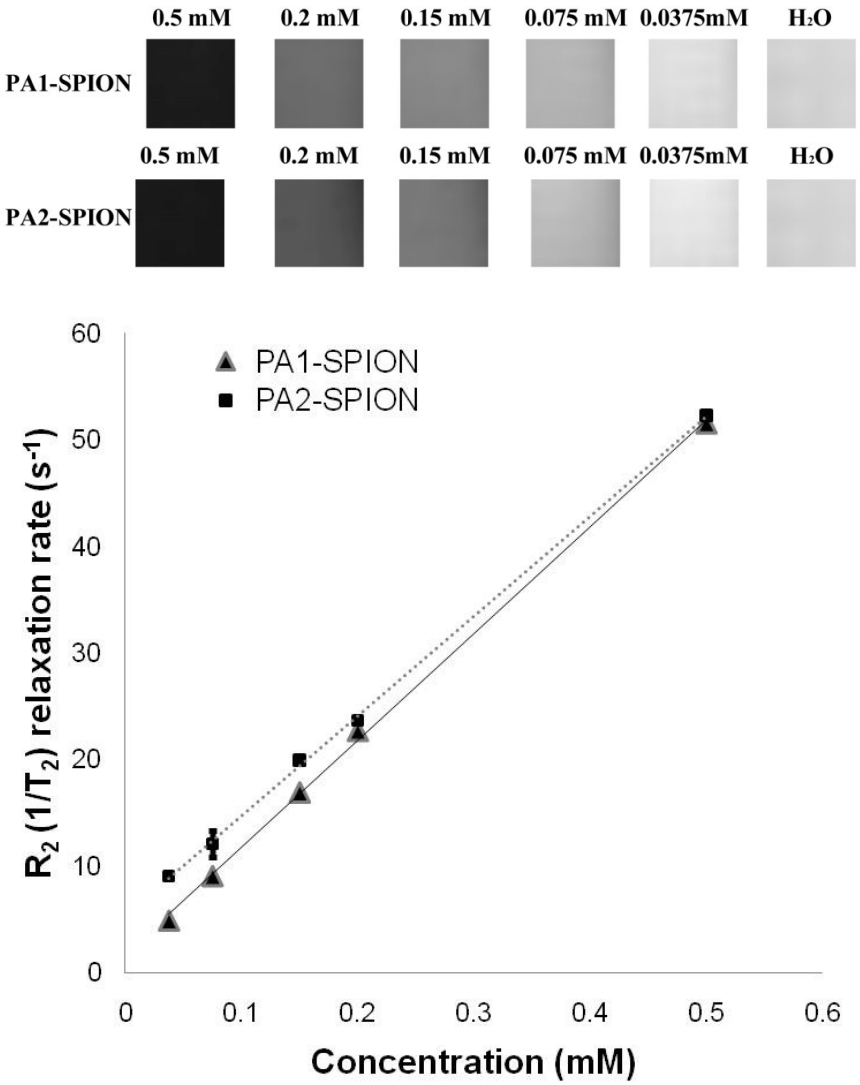

Figure 31. Contrast images of the peptide-SPION complexes measured at TR= 3000 ms and TE=50 ms (top). Relaxation rates (1/T2, s-1) of PA1-SPION and PA2-SPION versus iron concentration in water in a magnetic field of 3 T at room temperature (bottom). These images and graph demonstrate the efficiency of contrast agent, and their r2 transversal relaxivity were around 100,4 and 93,7 s-1mM-1 and their r2/r1 ratio were 111.55 and 55.1 for PA1-SPION and PA2-SPION, respectively.

Table 1. Physicochemical properties of peptide-SPION complexes

SPION coating	size by TEM (nm)	size by DLS (nm)	Transversal Relaxivity (r_2) ($s^{-1}mM^{-1}$)	r_2/r_1	Saturation Magnetization (M_s) (emu/g)
Lauric acid	7 nm	8-10 nm	---	---	53
P1	24 nm	24-32 nm	100.4	111.55	8
P2	30 nm	26-38 nm	93.7	55.1	5

3.4. Surface Modification of SPIONs with APTES molecules

Surfactant group attaches to the core of the iron oxide with coordination bond. As mentioned earlier, peptide-SPION is not stable in electrical field. Herein, we search for an alternative system in place of peptide-SPION complex. APTES modification is one of the best studied molecule forming water soluble SPIONs. Briefly, 10 mg SPION was diluted in 100 ml hexane and 0.5 ml APTES solution was added into the solution with 10 µL acetic

acid solutions. They were mixed and SPIONs were subsequently precipitated. They were washed with the help of magnet. After the washing step, they were characterized with FT-IR. The peak around 3400 cm^{-1} demonstrated the existence of APTES attached to the SPION surface (Figure 32) [6]. Size and zeta potential of the APTES-SPION were measured by DLS method. The hydrodynamic size of the particles was found to be 850 nm with a net surface potential at 3 mV (Figure 33-34). In other words, nanoparticles had a great tendency to aggregate due to the lack of the repulsive forces.

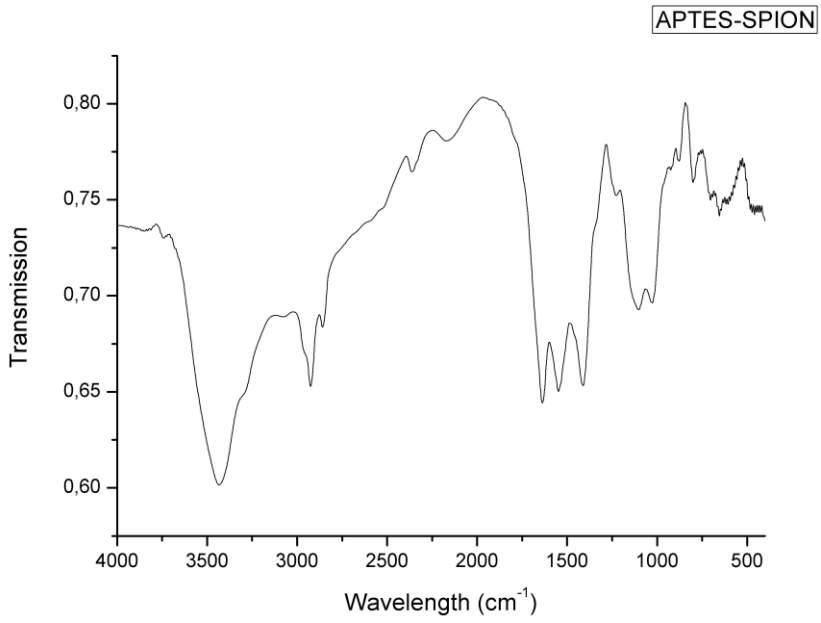

Figure 32. FT-IR spectrum graphic of APTES modified SPIONs. The existence of peak around 3400 cm-1 demonstrates the presence of APTES molecule.

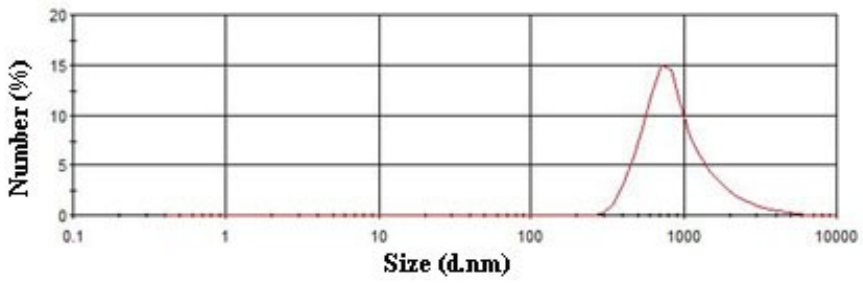

Figure 33. Hydrodynamic size of the APTES modified SPIONs measured with DLS. APTES modified SPION particle sizes were 800 nm, particles were agglomerated.

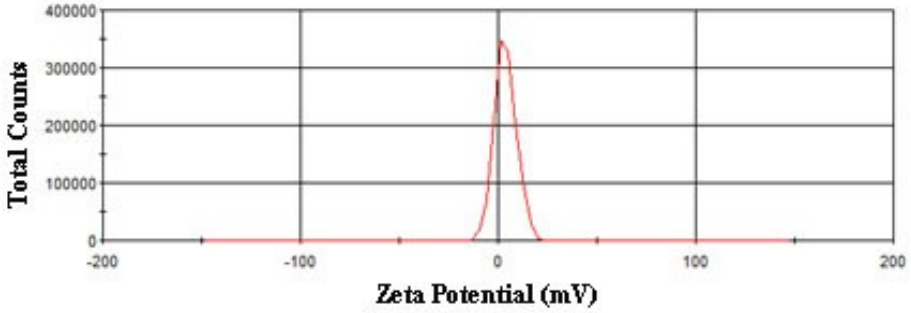

Figure 34. Zeta potential graphic of APTES modified SPIONs. Zeta Potential of the SPION was +3 mV. APTES-SPIONs had a great tendency to aggregate due to the lack of the repulsive forces.

3.5. Cellular Interaction of functionalized SPIONs

Cellular interactions of peptide-SPION complexes were characterized via several methods. Firstly, their biocompatibility was tested in vitro by culturing NIH 3T3 cells with them. Cell viability increased up to 170% compared with the negative control (Figure 35) when they incubated with peptide-SPION complex. Taking account these results, we can claim that peptide-SPION complexes are highly biocompatible. The reason of the

increased cell viability could be due to the peptide coating which provide nutrition and mechanical support for the cell in a similar way to natural extracellular matrix. To test this hypothesis, cell viability test was repeated with cells treated with only PA molecules and as clearly demonstrated in Figure 36, they again resulted in an increased cell viability.

To test the cellular interaction and localization, Prussian blue staining was performed. Staining was carried out after 24h of cell incubation in the presence of the PA-SPION complex. As can be seen from the inverted light microscope images of the cells incubated in the presence and absence of PA-SPION complexes (Figure 37), while positively charged **PA1**-SPIONs could be observed clearly as they located on the cell membrane or matrix, negatively charged **PA2**-SPION complexes couldn't bind to the cells and were removed in the washing step (Figure 37) showing no trace of the dye. In conclusion, positively charged molecules are electrostatically attracted to the cell membrane because of the negative charge of the cell surface.

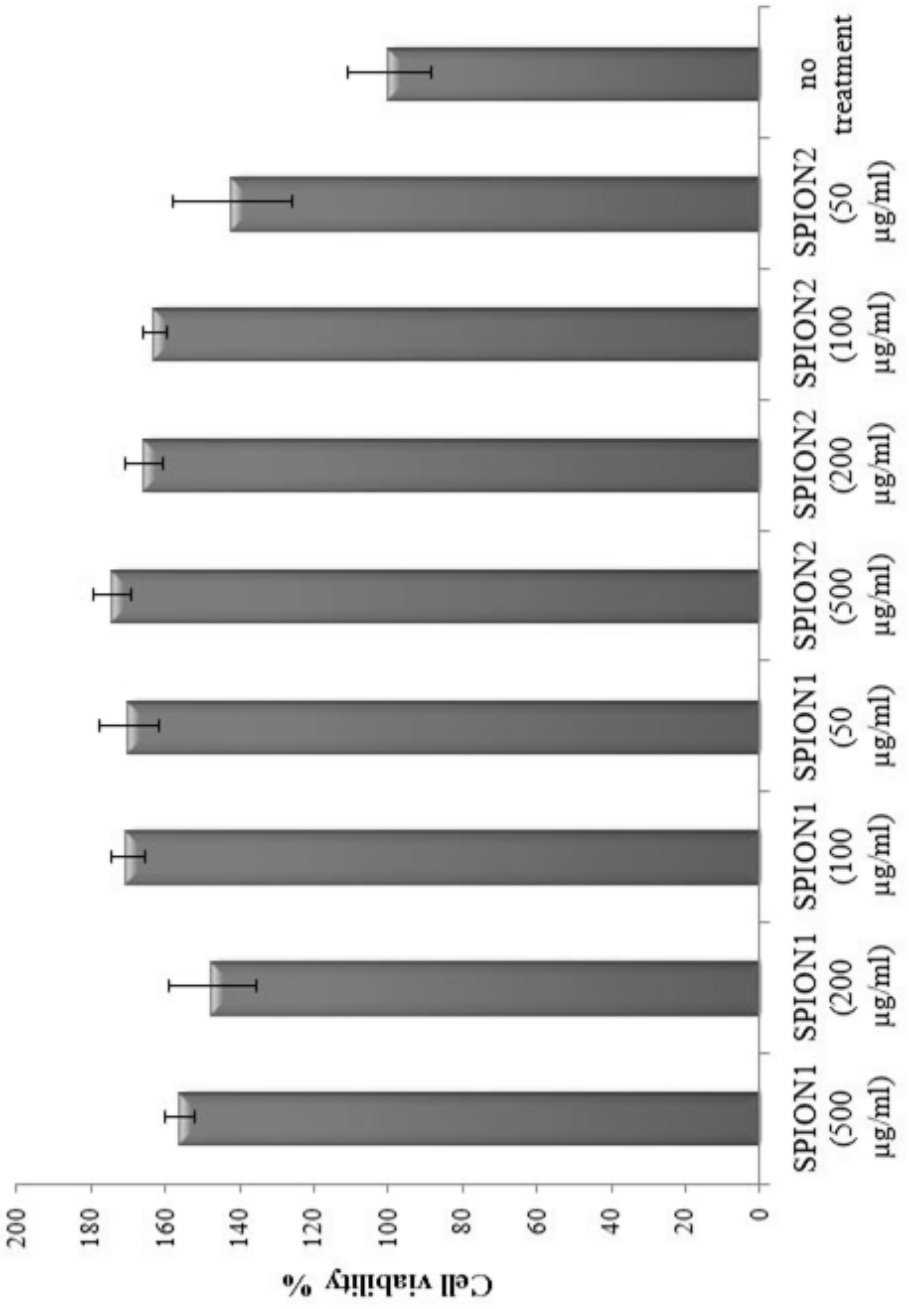

Figure 35. Cell Viability results of PA1-SPION and PA2-SPION incubated cells. Viability of the NIH3T3 cells incubated with SPIONs was increased up to 160 %.

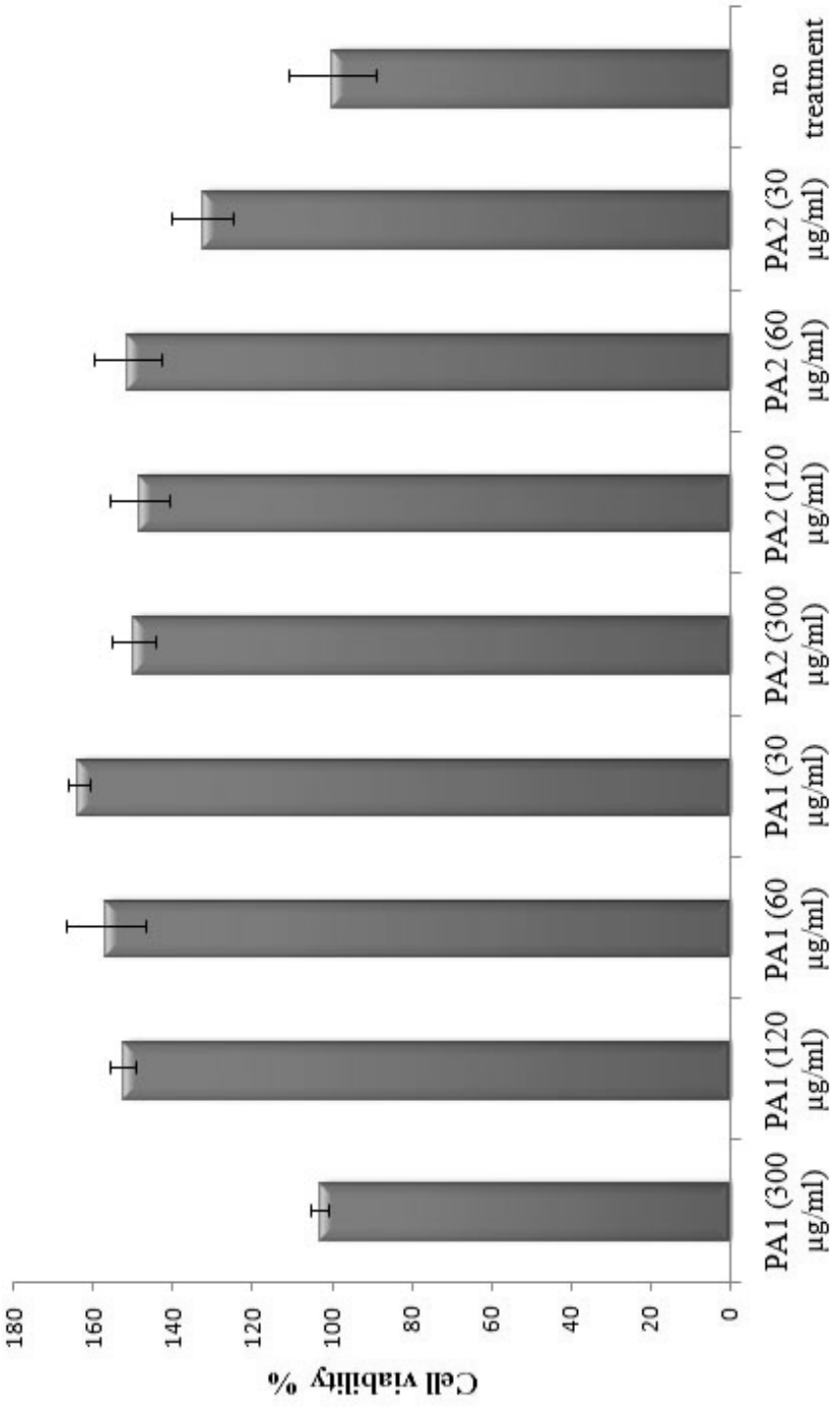

Figure 36. Cell viability result of PA1 and PA2 incubated cells. Viability of the NIH3T3 cells incubated with PA was increased.

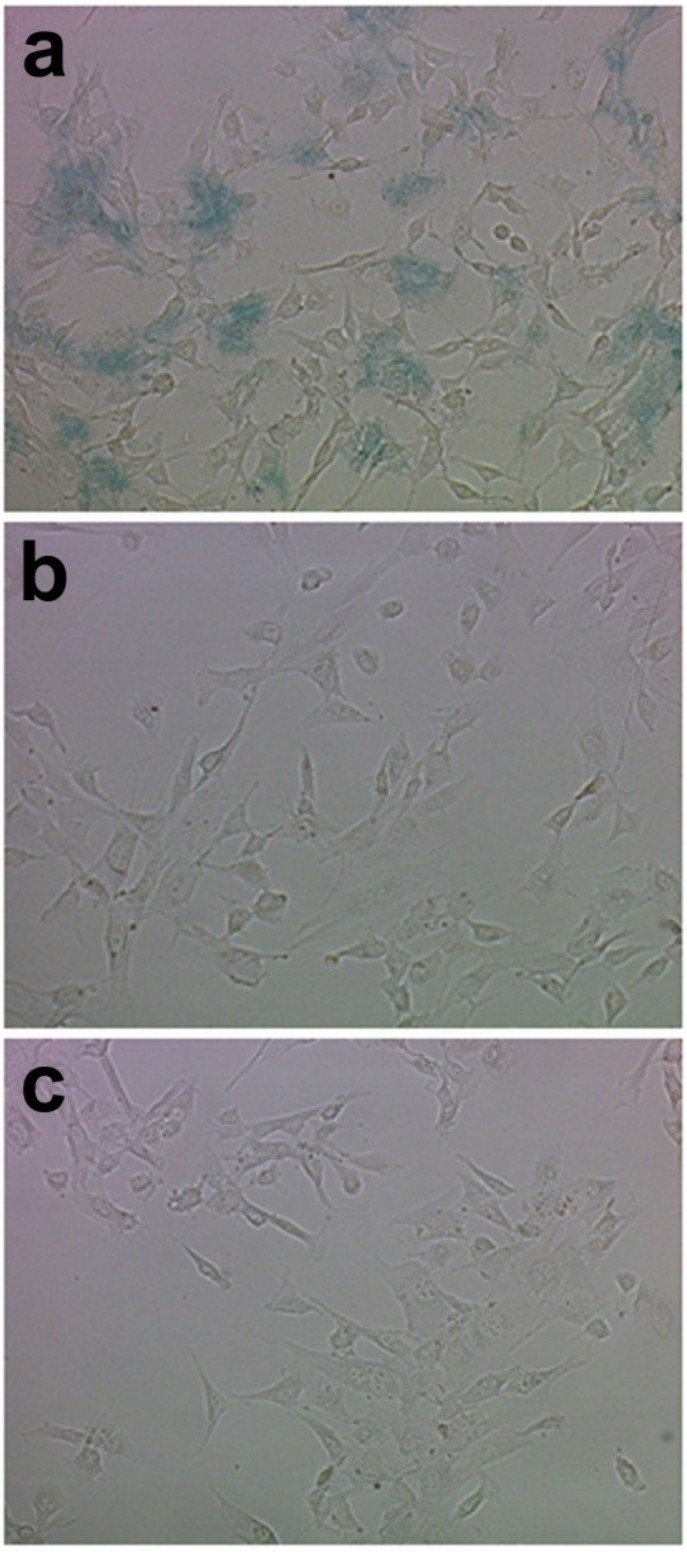

Figure 37. Cellular localization images of **a)** PA1-SPION **b)** PA2-SPION **c)** Negative Control. Positively charged SPIONs were located around cells whereas negatively charged SPIONs were removed at washing step.

3.6 Conjugation of SPIONs with Proteins

Targeted therapy and imaging is the feature direction of the medicine. Targeted molecules would not only increase the effectiveness of the carried molecules but also would decrease their side effects to the untargeted tissues or cells. Protein conjugation is one of the ways to target molecules into the desired area. In this study, we aimed to develop targeted superparamagnetic contrast agents modified with peptides. For that purpose, we conjugated streptavidin molecules with the PA2-SPION, and biotin with APTES modified SPIONs. Streptavidin has high affinity to biotin and they are often used for the protein conjugation studies. Thus, we attempted to conjugate proteins (Streptavidin or biotin) on SPION surface by EDC/NHS conjugation method. A representative diagram of conjugation studies with EDC/NHS reaction represented in Figure 38. EDC/NHS reaction has two distinctive steps. At the first step free carboxyl group interacted with EDC and NHS will stabilize the EDC group. This step has to be done at pH 5-6 where EDC mostly active. Then the activated molecule can be conjugated with a molecule that contains amine group. This step needs to be in a pH above 7 where EDC is in inactive form. Later, SPIONs are activated through EDC/NHS reaction and then conjugated with streptavidin molecules.

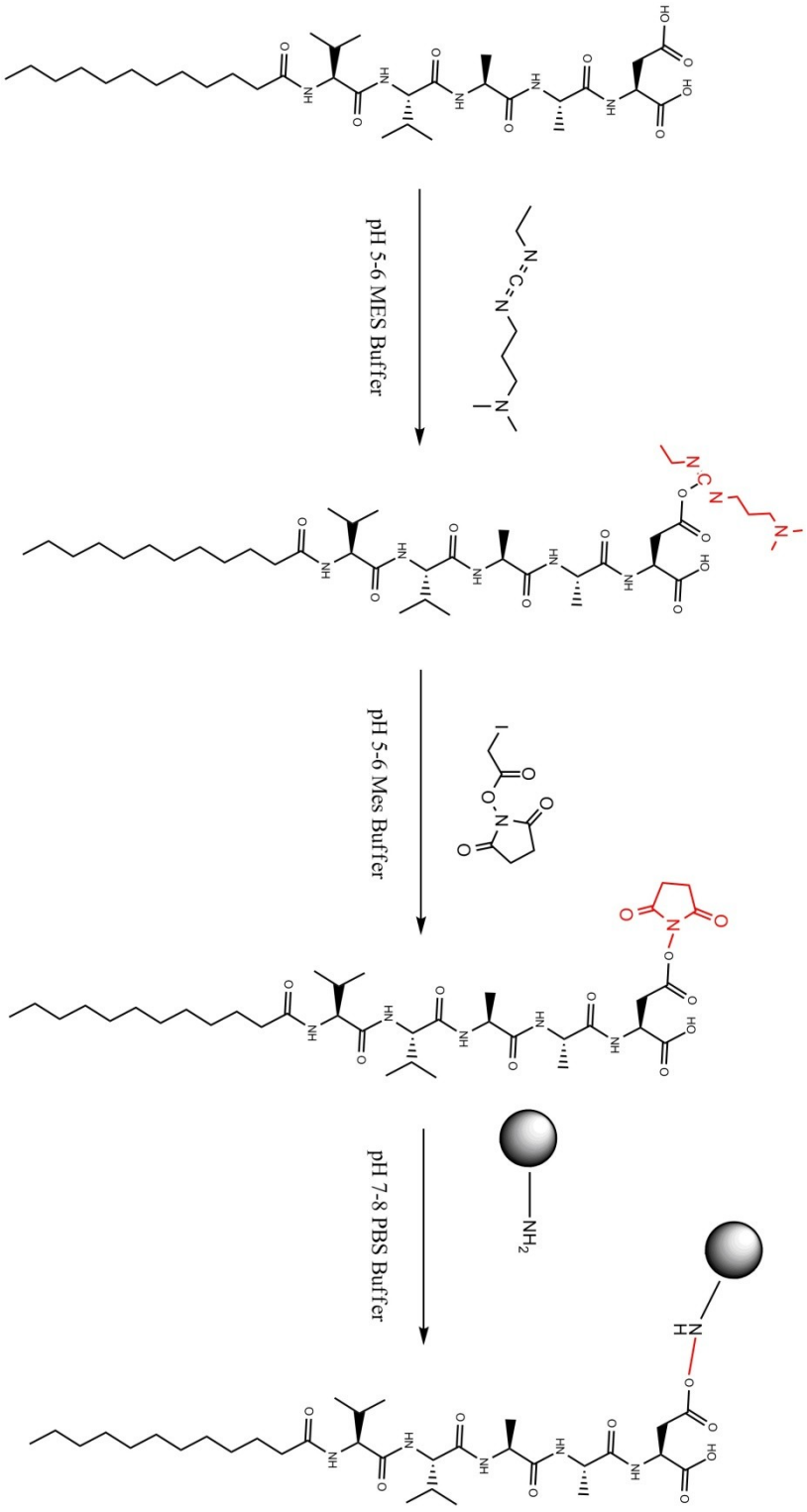

Figure 38. Representative scheme of conjugation studies. EDC binds to carboxyl groups, and then NHS stabilizes the complex. A molecule with amide group can be conjugated after carboxyl activation.

In this part of the study, Pro-PA(1) Pro-PA(2) was used instead of PA-1 and/or PA-2, since PA-1 and PA-2 can form self-assembled structures through non-covalent interactions. As mentioned above, protein conjugation needs to be done at different pHs, and these two peptide can agglomerate with each other leading a poor protein conjugation. To prevent this, we used proline amino acid which is known as hydrogen bond breaker. By this way, more stable particles could be achieved at different pH levels.

Pro-PA(1)-SPION complex were characterized using DLS method. Size and zeta potential of the Pro-PA(1)-SPION complex were 35 nm and -60 mV, respectively (Figure 39-40). After the protein conjugation, an increase in their size to 70 nm and 140 nm with a decreased zeta potential to -40 mV were observed as represented in Figure 41 and 42. These results were supported by the FT-IR outcomes represented in Figure 43 where a significant decrease in carboxyl peak at 1400 cm^{-1} corresponding to the protein conjugation was observed.

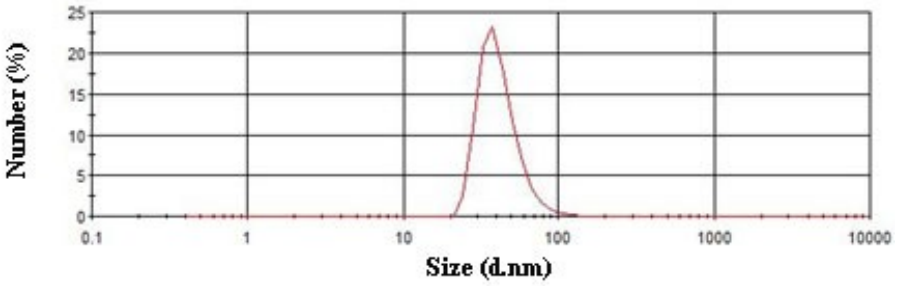

Figure 39. Hydrodynamic Size of the Pro-PA(1)-SPION complex measured with DLS. Hydrodynamic size of SPIONs was 35 nm.

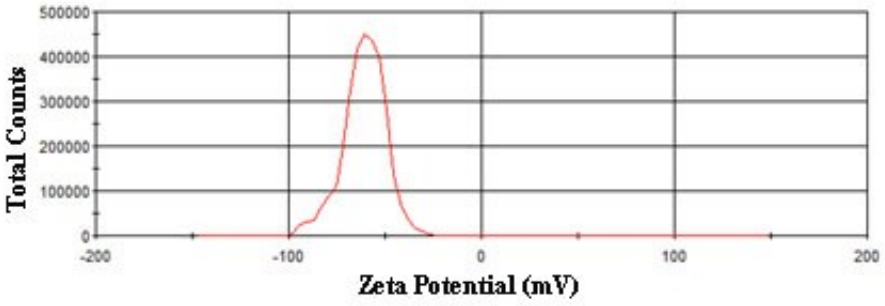

Figure 40. Zeta Potential graphic of Pro-PA(1)SPION complexes measured with DLS. Zeta potential of SPIONs was -60 mV.

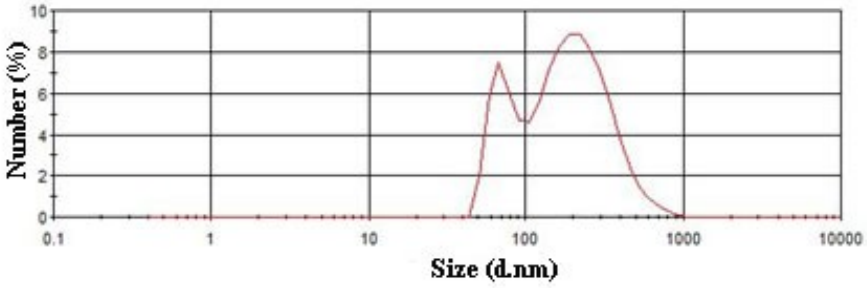

Figure 41. Hydrodynamic Size of the protein conjugated SPIONs measured with DLS. Hydrodynamic size of SPIONs was 80-180 nm. Hydrodynamic size of the SPION was increased after the conjugation.

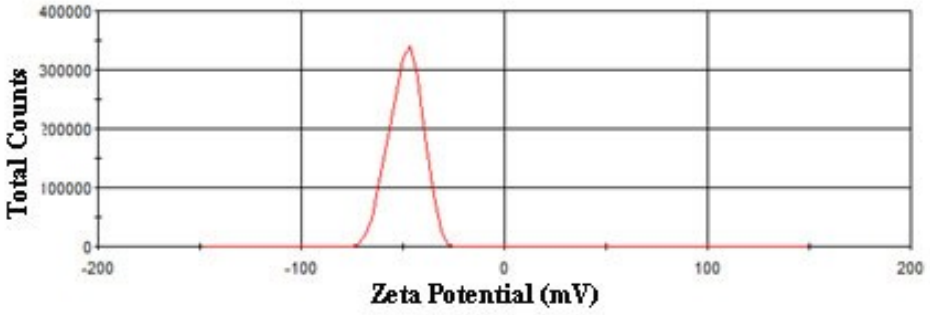

Figure 42. Zeta Potential graphic of protein conjugated SPIONs measured with DLS. Zeta potential of SPIONs was -40 mV. Zeta potential of the SPION was decreased after conjugation. This situation proves the success of conjugation process.

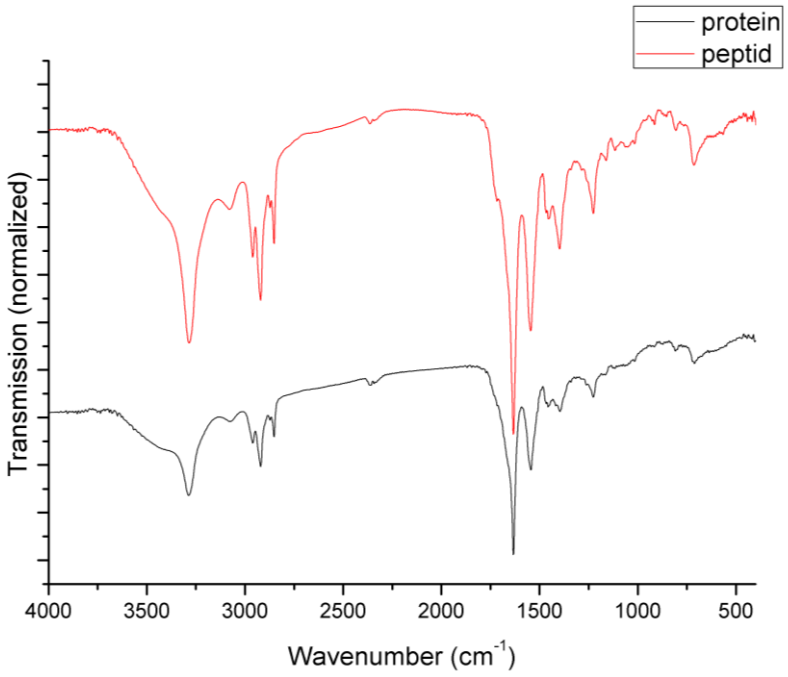

Figure 43. FT-IR spectrum of Pro-PA(1)-SPION and protein conjugated SPION. The peak located at 1400 cm-1 belongs to carboxyl group. There was significant decrease at carboxyl peak after streptavidin conjugation demonstrating a successful protein conjugation.

Protein conjugation was also studied with APTES modified SPIONs. Firstly, biotin was activated through EDC/NHS reaction. 1 mg biotin mixed with 11 mg EDC and 15 mg NHS in 5 ml MES buffer (0.1M, pH 5). This solution was mixed overnight, and then was left to conjugate through the amine groups of APTES. Before the conjugation reaction, hydrodynamic size of the APTES-SPION was found to be 850 nm whereas their zeta potential was 3 mV (Figure 44, 45). After the biotin conjugation, zeta potential of the SPIONs significantly decreased to -28 mV and their hydrodynamic size decreased to 110 nm. Nanoparticles are known to be more stable when they have zeta potential values around or higher than ±30

mV, thus, it could be claimed that stability of the SPIONs was increased after the biotin conjugation due to an increased surface net charge close to these boundaries. .

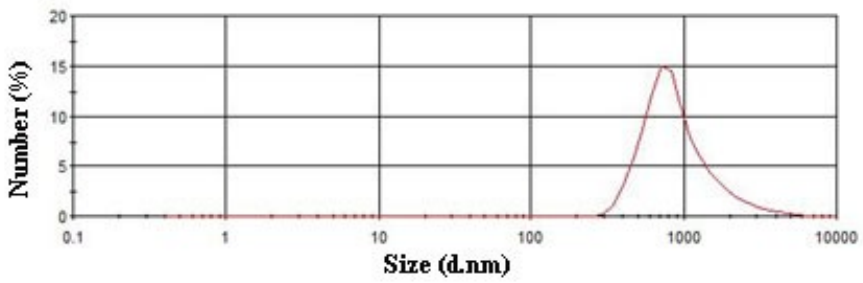

Figure 44. Hydrodynamic size of the SPIONs modified with APTES measured with DLS. Hydrodynamic size of the SPION was 800 nm. Particles were agglomerated.

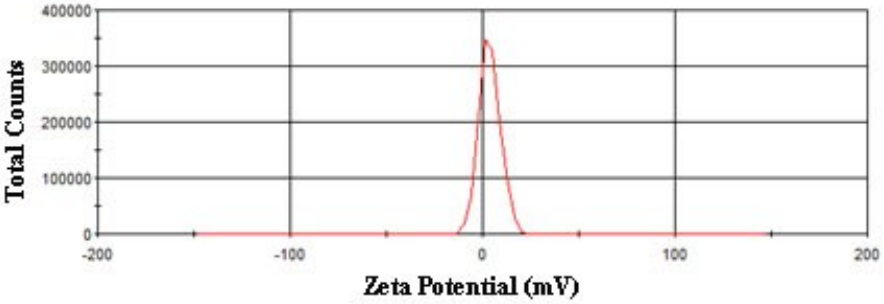

Figure 45. Zeta Potential graphic of SPIONS modified with APTES measured with DLS. Zeta potential of the APTES-SPION was +3 mV. Particles tend to agglomerate or aggregate.

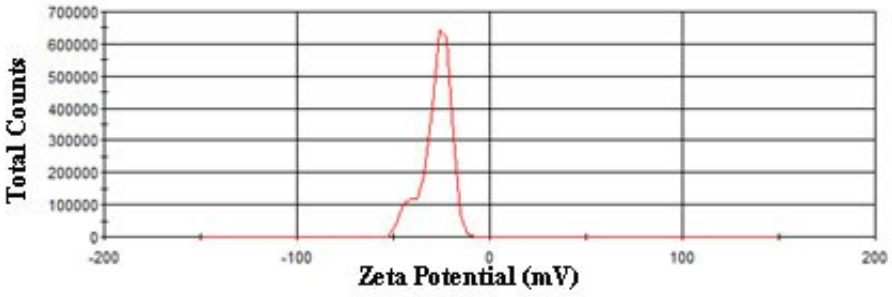

Figure 46. Zeta Potential graphic of biotin conjugated SPIONs measured with DLS. After the conjugation, the zeta potential of the complex was significantly changed and final zeta potential was -28mV.

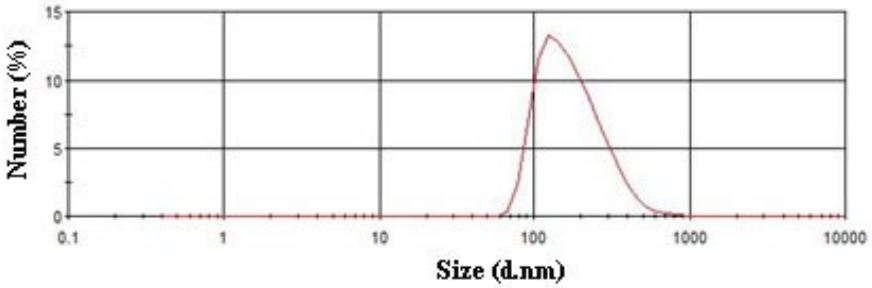

Figure 47. Hydrodynamic Size of the protein conjugated APTES-SPIONs measured with DLS. After the conjugation, the zeta potential of the complex was significantly decreased. Its zeta potential was around 110 nm.

Furthermore, conjugation process was also supported by FT-IR analysis. According to the results represented in Figure 48, changes in the free amine peak, especially, the existence of amide bond around 1560 cm^{-1}, is an indicator of the success of the conjugation process. Biotin conjugated SPIONs were also studied with fluorescence microscopy. Biotin conjugated SPIONs were mixed with FITC labeled streptavidin. After several washing step, complexes were analyzed with fluorescence microscopy. As can be seen in Figure 49, FITC labeled streptavidin interacts with biotinylated SPIONs.

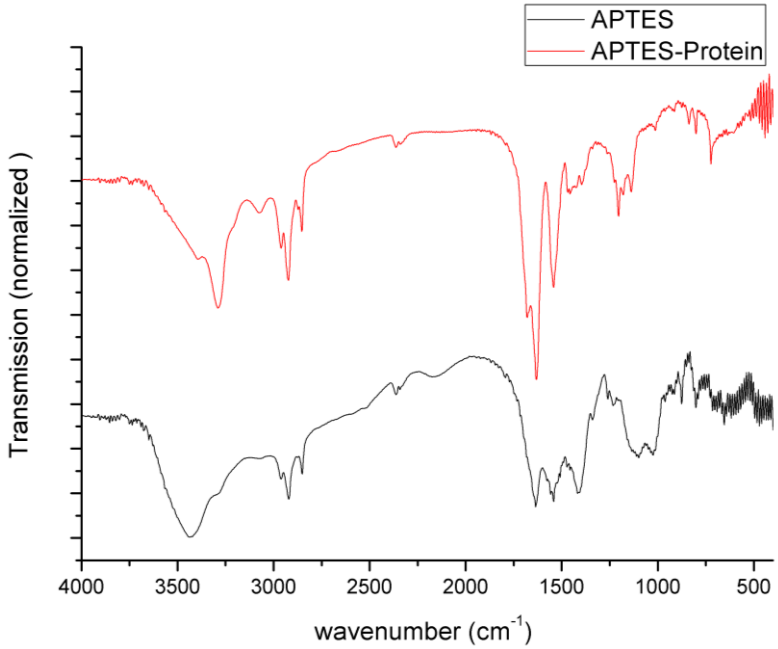

Figure 48. FT-IR graph of APTES modified and biotin conjugated SPIONs. After the protein conjugation, peaks were shifted to red region and an amide peak at 1560 cm^{-1} was observed.

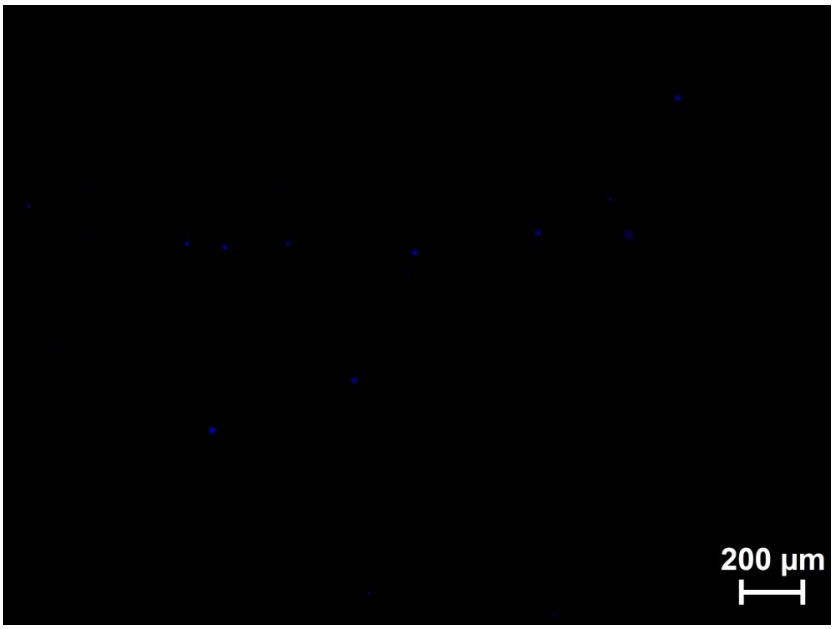

Figure 49. Fluorescence microscopy images of FITC labeled streptavidin biotin conjugated SPION interaction. Observed fluorescence shows that there are some the SPIONs conjugated with FITC labeled protein molecules

CHAPTER 4

CONCLUSIONS AND FUTURE DIRECTION

4.1. Conclusion

Several methods have been developed to synthesize SPIONs. In the first part of this study, comparison studies were carried out in order to find the best fitting method of SPION synthesis. SPIONs are exclusively produced by hydrolytic routes such as co-precipitation. The growth of iron oxide in aqueous media is controlled via large number kinetic factors. On account of this, widen particle size distribution was obtained using this method where the produced particles tend to aggregate in aqueous solutions. In contrast, another known method, thermal decomposition method, was shown to be overcoming these drawbacks of co-precipitation method by adopting pyrolysis rather than hydrolysis. In thermal decomposition method, the numbers of kinetic factors are greatly reduced and thus uniform SPIONs can easily be synthesized.

In thermal decomposition method; acids, amine bearing long hydrophobic tail molecules are used to coat SPIONs eventually provide them solubility in non-polar solvents. For their medical use, surface engineering has to be applied.

Herein, we developed a novel method for coating SPIONs based on the intercalation of PA molecules with SPIONs by hydrophobic interactions. The hydrophobic encapsulation of SPIONs by PA molecules provided solubility in water and enabled us to overcome problems associated with the surfactant exchange for SPION coating such as changes in crystallinity, synthesis efficiency, and conformational changes in proteins.

Peptide amphiphile molecules provide stability to SPIONS in aqueous solutions due to their amphiphilic character. Moreover, an incremented biofunctionality based on the peptide sequence and enhanced physicochemical properties of SPIONs could be achieved by the peptide coating. Also SPPS protocol enables control over peptide sequences [31] for more specific and selective localization of nanoparticles to target cells. By using homing peptide sequences [32], it is possible to target SPIONs to the organs such as brain [33], kidney [33], hearth [34], breast [32] and several other tumor tissues [35,36]. Thus, by using non-covalent functionalization of SPIONs with appropriate peptide sequences, cellular or molecular targeting is possible without any further coupling process. There are specific molecular tags, so called “zip codes” that can be specifically over-regulated either by normal or abnormal organs or tissues, such as cancer tissues. These zip codes can be recognized by specific homing proteins or peptides.

To improve the signal to noise ratio, contrast agents have to be used. In this study, use of peptide-SPION complex as MRI contrast agent was also studied. There are several factors have to be taken into consideration for a

good contrast agent which are size of the nanoparticles, magnetization values of nanoparticles as well as r_2 values, r_2/r_1 values and biocompability. The size of the nanoparticles was around 35 nm which is acceptable for biological uses. The magnetization values of the peptide-SPION complex (PA1-SPION and PA2-SPION) were in a sufficient range for their use in biological applications. The efficiency of the contrast agents are determined mostly with r_2 and r_2/r_1 ratio. In this study, r_2 values of PA1-SPION and PA2-SPION were 100.4 and 93.7 $mm^{-1}s^{-1}$ respectively which are very close to commercial examples as stated above. The r_2/r_1 ratio was much greater than the commercial examples. *In vitro* cell culture experiments on NIH 3T3 cells revealed that the peptide-SPION complex promises biocompatible feature.

Briefly, we developed a new method to synthesize a biofunctional and biocompatible material. The synthesis protocol consists of just mixing the material in appropriate conditions. As mentioned above MR active system shown here can be selectively functionalized by using various peptide molecules for targeting specific tissues.

Protein conjugation was also studied with these complexes. Several methods have been used for the protein conjugation. EDC/NHS reaction was used for the conjugation studies. Pro-PA(1) and Pro-PA(2) SPION complexes and APTES modified nanoparticles complexes were incubated with protein molecules both type of particles were successfully synthesized. These studies are still in progress.

Whilst SPIONs have tremendous potential in a wide range of applications, to date problems in their stability has limited the wide-spread use of them. In this direction, the present thesis is a contribution to the optimization of a rapid and efficient method of SPION preparation and surface modification, and explores their potential as MRI contrast agent.

4.2 Future Direction

SPIONs can also be functionalized with various molecules such as proteins for the targeted therapy and diagnosis. Herein, we also demonstrate protein conjugation studies which can also be used for the targeted imaging. Conjugation was studied with peptide-SPION and APTES-SPION complexes. Although, peptide-SPION complex offers great feature with mimicking procedure, to increase the selectivity and specificity protein can be conjugated with amphiphilic peptides.

APTES covalently attached to SPIONs. SPION complex gained durability in different circumstances; they tend to aggregate, though. On account of that, purification and isolation of SPIONs are much easier than the peptide-SPION complex. The self-assembly on peptide-SPION will be studied. Self-assembled system is a new era in nanomedicine especially in tissue engineering and delivery applications. Tissues need unique cell scaffolds which have unique chemical and mechanotransduction properties. The chemical factors can be supplied with the peptide that is synthesized with SPPS protocol. SPIONs offer tremendous future for the tissue engineering applications. Rheological and optical properties of peptide-

SPION complex will be studied. Rheological properties of peptide-SPION complex represent their mechanical properties which are necessary information for tissue engineering process and drug delivery system. Their self-assembly feature will also be studied with circular dichroism. The gel formation will be visualized with SEM TEM and AFM.

Directed assembly with peptide-SPION will also be studied. Under the magnetic field these SPIONs can be formed aligned structure. Herein a unique magnet will be developed and peptide-SPION complex will be located on them.

For therapeutic applications and other imaging properties, we are working on a peptide coated magnetite and dye doped silica nanoparticles. We are also working on a polymer and peptide coated SPION complexes.

REFERENCES

(1) Vijay K. Varadan, L. C., Jining Xie *Nanomedicine: Design and Applications of Magnetic Nanomaterials, Nanosensors and Nanosystems*; wiley, 2008.

(2) Arruebo, M.; Fernández-Pacheco, R.; Ibarra, M. R.; Santamaría, J. *Nano Today* **2007**, *2*, 22.

(3) Kumar, C. S. S. R. *Magnetic Nanomaterials*; wiley, 2009.

(4) Gubin, S. P. *Magnetic Nanoparticles*; wiley-vch, 2009.

(5) NDT, r. c.; center, N. r., Ed.; NDT resource center.

(6) Lu, A.-H.; Salabas, E. L.; Schüth, F. *Angewandte Chemie International Edition* **2007**, *46*, 1222.

(7) Jun, Y.-w.; Lee, J.-H.; Cheon, J. *Angewandte Chemie International Edition* **2008**, *47*, 5122.

(8) Gupta, A. K.; Gupta, M. *Biomaterials* **2005**, *26*, 3995.

(9) Schladt, T. D.; Schneider, K.; Schild, H.; Tremel, W. *Dalton Transactions* **2011**, *40*, 6315.

(10) Sun, S.; Zeng, H.; Robinson, D. B.; Raoux, S.; Rice, P. M.; Wang, S. X.; Li, G. *Journal of the American Chemical Society* **2003**, *126*, 273.

(11) Laurent, S.; Forge, D.; Port, M.; Roch, A.; Robic, C.; Vander Elst, L.; Muller, R. N. *Chemical Reviews* **2008**, *108*, 2064.

(12) Elimelech, M.; Gregory, J.; Jia, X.; Williams, R. A.; Gregory, J.; Jia, X.; Williams, R. A. In *Particle Deposition & Aggregation*; Butterworth-Heinemann: Woburn, 1995, p 33.

(13) Malvern http://www.malvern.com/LabEng/industry/colloids/dlvo_theory.htm

(14) Sun, C.; Lee, J. S. H.; Zhang, M. *Advanced Drug Delivery Reviews* **2008**, *60*, 1252.

(15) Na, H. B.; Song, I. C.; Hyeon, T. *Advanced Materials* **2009**, *21*, 2133.

(16) Zhou, L.; Yuan, J.; Wei, Y. *Journal of Materials Chemistry* **2011**, *21*, 2823.

(17) Wang, G.; Su, X. *Analyst* **2011**, *136*, 1783.

(18) Brown, M. A. a. S., R. C *MRI: Basic Principles and Applications*; 3.rd ed.; Wiley: Hoboken: New York, 2005.

(19) Qiao, R.; Yang, C.; Gao, M. *Journal of Materials Chemistry* **2009**, *19*, 6274.

(20) EMRIC. http://www.cardiff.ac.uk/biosi/researchsites/emric/

(21) De Palma, R.; Peeters, S.; Van Bael, M. J.; Van den Rul, H.; Bonroy, K.; Laureyn, W.; Mullens, J.; Borghs, G.; Maes, G. *Chemistry of Materials* **2007**, *19*, 1821.

(22) van Oss, C. J. In *Interface Science and Technology*; Carel, J. v. O., Ed.; Elsevier: 2008; Vol. Volume 16, p 31.

(23) Srinivasan, B.; Huang, X. *Chirality* **2008**, *20*, 265.

(24) Tartaj, P.; Serna, C. J. *Journal of the American Chemical Society* **2003**, *125*, 15754.

(25) Scopes, R. K. *Analytical Biochemistry* **1974**, *59*, 277.

(26) Mailänder, V.; Landfester, K. *Biomacromolecules* **2009**, *10*, 2379.

(27) Weissleder, R.; Stark, D. D.; Engelstad, B. L.; Bacon, B. R.; Compton, C. C.; White, D. L.; Jacobs, P.; Lewis, J. *Am. J. Roentgenol.* **1989**, *152*, 167.

(28) Wang, L.; Neoh, K. G.; Kang, E. T.; Shuter, B.; Wang, S.-C. *Advanced Functional Materials* **2009**, *19*, 2615.

(29) Reimer, P.; Rummeny, E. J.; Daldrup, H. E.; Balzer, T.; Tombach, B.; Berns, T.; Peters, P. E. *Radiology* **1995**, *195*, 489.

(30) Jung, C. W.; Jacobs, P. *Magn. Reson. Imaging* **1995**, *13*, 661.

(31) W. C. Chan , P. D. W. *Fmoc Solid Phase Peptide Synthesis A Practical Approach*; oxford university press inc.: new york, 2004.

(32) Essler, M.; Ruoslahti, E. *Proceedings of the National Academy of Sciences of the United States of America* **2002**, *99*, 2252.

(33) Pasqualini, R.; Ruoslahti, E. *Nature* **1996**, *380*, 364.

(34) Zhang, L.; Hoffman, J. A.; Ruoslahti, E. *Circulation* **2005**, *112*, 1601.

(35) Arap, W.; Pasqualini, R.; Ruoslahti, E. *Science* **1998**, *279*, 377.

(36) Pasqualini, R.; Koivunen, E.; Kain, R.; Lahdenranta, J.; Sakamoto, M.; Stryhn, A.; Ashmun, R. A.; Shapiro, L. H.; Arap, W.; Ruoslahti, E. *Cancer Research* **2000**, *60*, 722.